

Review

# A Geoscientific Review on CO and CO<sub>2</sub> Ices in the Outer Solar System

Caitlin Ahrens<sup>1,\*</sup>, Hypatia Meraviglia<sup>2</sup> and Christopher Bennett<sup>3</sup><sup>1</sup> Solar System Exploration Division, NASA Goddard Space Flight Center, Greenbelt, MD 20771, USA<sup>2</sup> Department of Physics and Astronomy, University of Central Arkansas, Conway, AR 72035, USA; hbarry@cub.uca.edu<sup>3</sup> Department of Physics, University of Central Florida, Orlando, FL 32816, USA; Christopher.Bennett@ucf.edu

\* Correspondence: Caitlin.ahrens@nasa.gov

**Abstract:** Ground-based telescopes and space exploration have provided outstanding observations of the complexity of icy planetary surfaces. This work presents our review of the varying nature of carbon dioxide (CO<sub>2</sub>) and carbon monoxide (CO) ices from the cold traps on the Moon to Pluto in the Kuiper Belt. This review is organized into five parts. First, we review the mineral physics (e.g., rheology) relevant to these environments. Next, we review the radiation-induced chemical processes and the current interpretation of spectral signatures. The third section discusses the nature and distribution of CO<sub>2</sub> in the giant planetary systems of Jupiter and Saturn, which are much better understood than the satellites of Uranus and Neptune, discussed in the subsequent section. The final sections focus on Pluto in comparison to Triton, having mainly CO, and a brief overview of cometary materials. We find that CO<sub>2</sub> ices exist on many of these icy bodies by way of magnetospheric influence, while intermixing into solid ices with CH<sub>4</sub> (methane) and N<sub>2</sub> (nitrogen) out to Triton and Pluto. Such radiative mechanisms or intermixing can provide a wide diversity of icy surfaces, though we conclude where further experimental research of these ices is still needed.



**Citation:** Ahrens, C.; Meraviglia, H.; Bennett, C. A Geoscientific Review on CO and CO<sub>2</sub> Ices in the Outer Solar System. *Geosciences* **2022**, *12*, 51. <https://doi.org/10.3390/geosciences12020051>

Academic Editors: Simon Wing, Philippe Claeys and Jesus Martinez-Frias

Received: 6 December 2021

Accepted: 10 January 2022

Published: 20 January 2022

**Publisher's Note:** MDPI stays neutral with regard to jurisdictional claims in published maps and institutional affiliations.



**Copyright:** © 2022 by the authors. Licensee MDPI, Basel, Switzerland. This article is an open access article distributed under the terms and conditions of the Creative Commons Attribution (CC BY) license (<https://creativecommons.org/licenses/by/4.0/>).

**Keywords:** ices; frost lines; outer solar system; Galilean satellites; Saturn system

## 1. Introduction

Carbon-bearing (C-bearing) species are common throughout the Solar System, with the most abundant species observed in comets and planetary surfaces being carbon dioxide (CO<sub>2</sub>), followed by carbon monoxide (CO), and methanol (CH<sub>3</sub>OH) [1,2]. CO<sub>2</sub> and CO have been observed (or inferred) through spectroscopic observations, either through ground-based and space telescopes, like the Spitzer Space Telescope, Infrared Astronomical Satellite (IRAS), United Kingdom Infrared Telescope (UKIRT), or planetary missions, such as Galileo, Voyager 2, and New Horizons. Such missions provided images and spectroscopic data whose absorption bands have been used to determine the nature of CO<sub>2</sub> and CO solids (see Section 3). Interestingly, the CO<sub>2</sub> band positions shift on the various planetary bodies, connoting the complex and variable nature in which the CO<sub>2</sub> solids are formed and mixed with other species on these icy surfaces.

In the Jovian and Saturnian systems, CO<sub>2</sub> on the surface of their satellites has a spectral band center wavelength consistent with a characteristic of solid CO<sub>2</sub> but not of the crystalline or amorphous phases, indicating a complexity with other materials, which may include water ice, H<sub>2</sub>O, and carbonaceous materials [3–5]. The slight blueshift of around 4–13 cm<sup>-1</sup> (observed for Ganymede, Callisto, Phoebe, Iapetus, and Hyperion) of the ν<sub>3</sub> band is thought to be associated with the CO<sub>2</sub> surrounded by a clathrate cage, which may be formed from a host ice, such as water or even non-ice material [3]. This is consistent with the fact that at the typical temperatures (e.g., ~100–160 K) and pressures of the Jovian and Saturnian satellites (10–100 s of μPa), pure CO<sub>2</sub> ice would otherwise sublimate away if not replenished frequently since its equilibrium vapor pressure is ~10<sup>-4</sup> to 10 Torr [6].

Iapetus demonstrates a good example of how CO<sub>2</sub>-type volatile mixing correlates with spectral shifting (see also Section 3), where the mixture with H<sub>2</sub>O shifts the CO<sub>2</sub> ν<sub>3</sub> band by confining the asymmetric stretching mode of the molecule (Figure 1) [7].

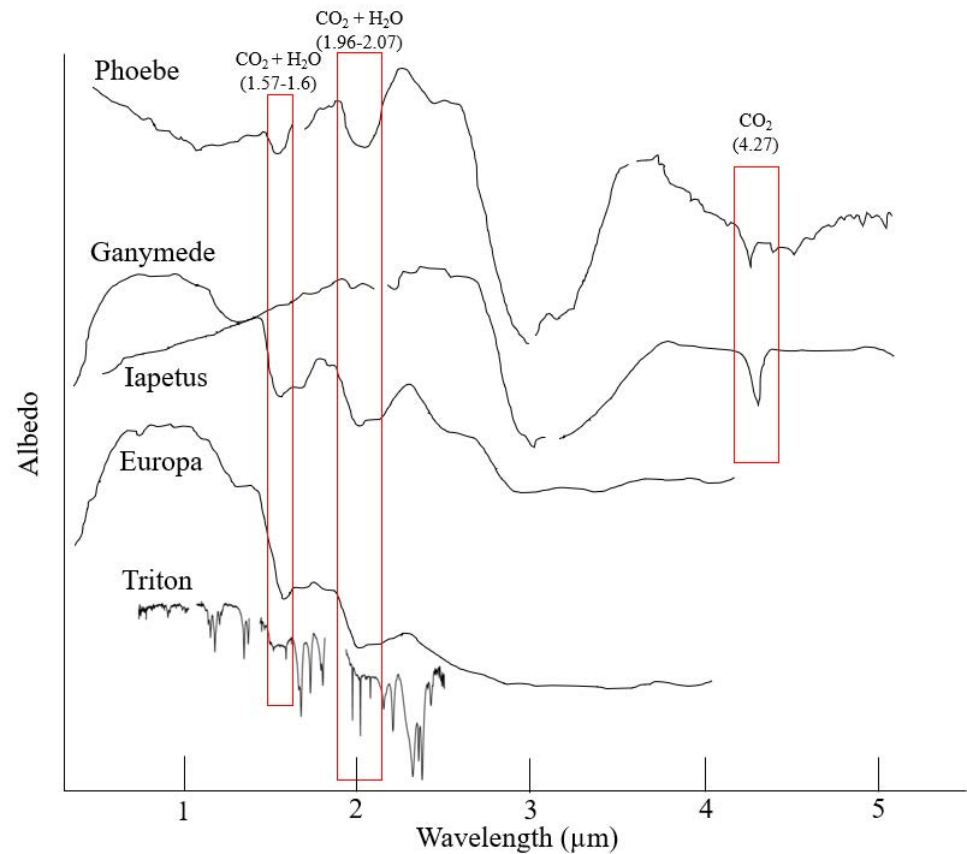


**Figure 1.** Infrared spectra of the Jovian, Saturnian, and Triton moons with labeled CO<sub>2</sub> (1.65, ~2.0, 4.27 μm) spectral bands. Note that the 4.27 μm band of Iapetus is shifted in comparison with the Phoebe spectrum. Spectra offset for clarity. Europa and Ganymede spectra from [8]; Iapetus spectrum from [9]; Phoebe spectrum from [10]; Triton spectrum from [11].

While the focus of this review focuses mostly on the outer Solar System beyond the asteroid belt, we should also briefly review the case for solid CO<sub>2</sub> on the Moon and Mars (and potentially within the craters of Mercury) [12]. The CO<sub>2</sub> placement in these inner rocky bodies serves as an interesting placement of CO<sub>2</sub> condensation and sublimation dynamics. On the Moon, particularly at the lunar poles, there are cold regions with temperatures < 110 K, as observed by the Diviner radiometer instrument onboard the Lunar Reconnaissance Orbiter (LRO) [13]. Free carbon, even observed in meteoritic samples, has no gaseous phase at lunar surface temperatures and therefore cannot condense, leaving CO<sub>2</sub> as the primary carbon constituent at lunar cold traps [2]. Pockets of CO<sub>2</sub> should be stable within certain craters, such as Haworth, Amundsen (Figure 2a), de Gerlache, and others, over a cumulative area of ~200 km<sup>2</sup> [2]. The confirmation of CO<sub>2</sub> volatiles at the lunar poles was also confirmed by the LCROSS (Lunar Crater Observation and Sensing Satellite) probe, which impacted within the Cabeus crater and released CO<sub>2</sub>, validating thermal stability models [14]. CO was also observed by the LRO Lyman Alpha Mapping Project (LAMP) instrument, though this may have been a case of CO being a decomposition product of the CO<sub>2</sub> released during the LCROSS impact [15]. The origin of this CO<sub>2</sub> is likely to be of solar wind origin [16] or micrometeoroids [1]. The sublimation rate of solid CO<sub>2</sub> at these cold traps would be negligible [2,17]. Exosphere models have observed that the capture rate of CO<sub>2</sub> on the Moon is rather high (compared to other volatiles), probably due to the low photodestruction rate of CO<sub>2</sub> in the gaseous state [18]. The age of the

lunar cold traps has been estimated to be  $\sim 2$  Gyr, with an accumulation of  $\text{H}_2\text{O}$  ice being  $50\text{--}500 \text{ kg/m}^2/\text{Gyr}$ , with the rate of  $\text{CO}_2$  accumulations proposed to be similarly high [2].

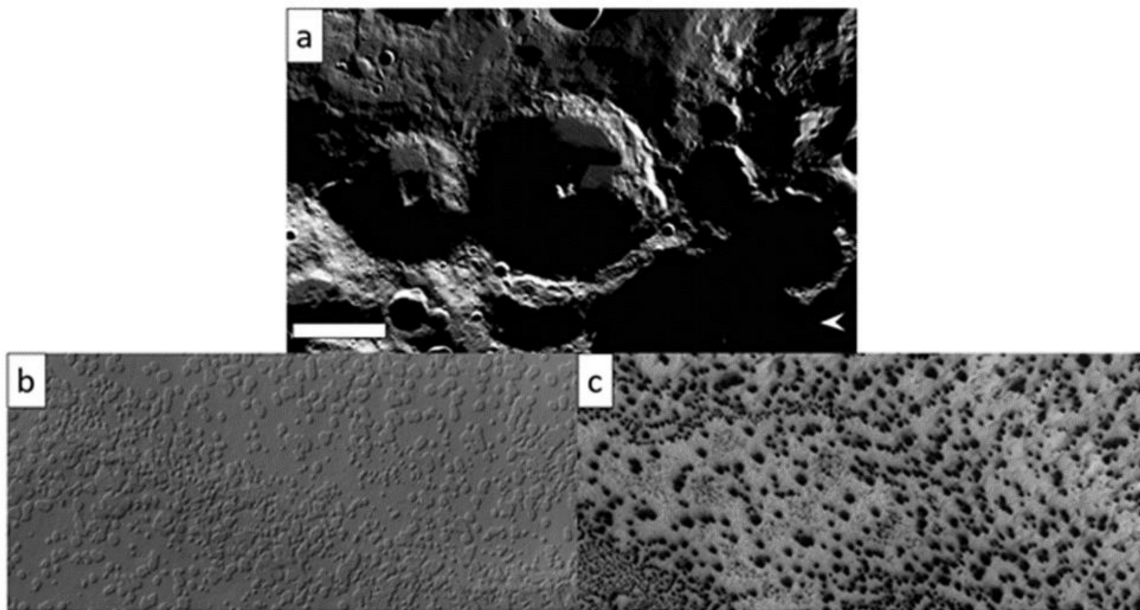


**Figure 2.** The lunar and Martian  $\text{CO}_2$ -rich geologic features. (a) Amundsen crater on the lunar south pole as imaged by the LRO Wide-angle Camera (WAC) has been observed to have stable  $\text{CO}_2$  volatiles within its shadowed crater walls [2]. Scale bar at 50 km; (b) Swiss cheese terrain from the southern Martian poles as imaged by HiRISE (ESP-012271-0940); (c)  $\text{CO}_2$  “spider” geysers on the Martian surface imaged by HiRISE (ESP-012643-0945). Both HiRISE images are 5 km across.

The detection of ice in the permanently shadowed craters of Mercury has been known since full-disk radar mapping of its surface was carried out by [19]. It is thought that most of the ice surviving in these craters has been accumulated through exogenous delivery in a similar manner as proposed for the Moon, where  $\text{CO}_2$  would be transported to these regions alongside other volatiles, such as  $\text{H}_2\text{O}$ , methane ( $\text{CH}_4$ ), and ammonia ( $\text{NH}_3$ ) [12].

The Mars Reconnaissance Orbiter (MRO) imaging and the Shallow Radar soundings have observed  $\text{CO}_2$  ice within the polar caps on Mars [20]. The Martian northern polar cap is shaped mostly by ice sublimation, deposition, and wind erosion [21], while the southern polar  $\text{CO}_2$  cap has distinctive pitting (a.k.a. “Swiss cheese”; Figure 2b) and  $\text{CO}_2$  geysers (a.k.a. “Spiders”; Figure 2c) produced by outgassing solid-state greenhouses [22,23]. Early in Mars’ geologic history,  $\text{CO}_2$  is thought to have been present at the  $\sim 1$  bar level ( $< 2$  m depth) and is likely stored in these polar layered deposits [20]. While these deposits are water-ice-dominated, the perennial  $\text{CO}_2$ -ice deposits are  $< 5$  m thick (amounting to an area of  $\sim 90,000 \text{ km}^2$ ) [20].

The outer Solar System hosts a complexity of volatiles and water ice, mostly located on the outer four planets beyond the water ice snow line  $\sim 2.7$  AU from the Sun, where radiation equilibrium temperature drops below 150 K. In this paper, we review the varying nature of the  $\text{CO}_2$  and CO ices from Jupiter to Pluto (Figure 3). The nature of  $\text{CO}_2$  on the surfaces of satellites around Jupiter and Saturn depends on the magnetospheric nature of their giant host planets, along with the relationship with water ice (Figure 3). It is also worth noting that the majority of the moons discussed here are tidally locked to their host planets, which themselves have extensive magnetospheres and short rotation periods. As a result, these moons typically have rotational periods close to their orbital periods whereby the same surface is always facing the host planet. The energetic electrons and ions within these magnetospheres therefore primarily interact with the trailing hemisphere for all but the

most energetic particles [24]. On the other hand, the leading hemispheres are more prone to space weathering by micrometeoroid impacts.

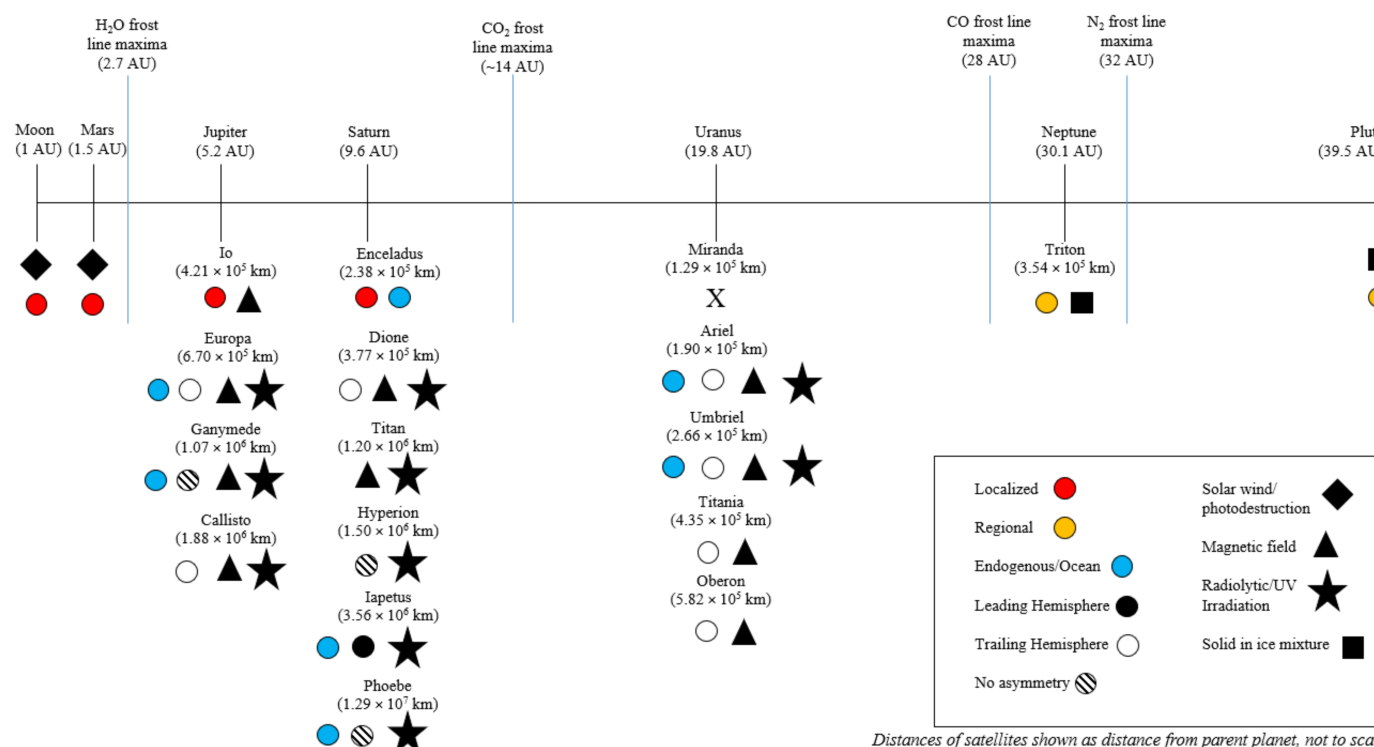


**Figure 3.** Map of the Solar System (in this review) regarding presence of CO<sub>2</sub> or CO on the surface (or subsurface), and possible environmental interactions at each satellite, such as magnetic fields or irradiation. Note that CO<sub>2</sub> is usually found on both trailing and leading hemispheres of these icy satellites, we mark the strongest presence of CO<sub>2</sub> here.

Uranus and Neptune are comparatively poorly understood due to the limiting data from Voyager 2. However, previous and current spectroscopic data from ground-based telescopes have helped our understanding of the CO<sub>2</sub> ices on only some (not all) of the Uranian moons, as well as their intermixed relationship with other ices, including CO, on Triton at Neptune. With minimal surface pressures, CO<sub>2</sub> is susceptible to sublimation, except on Triton, where surface temperatures are too low to drive CO<sub>2</sub> removal via sublimation [25]. Pure CO<sub>2</sub> ice is unstable over the age of the Solar System in the Jupiter-Uranus systems, and any detectable deposits of pure CO<sub>2</sub> must be actively synthesized, delivered, or recently exposed by impacts, tectonism, or emplaced by cryovolcanism [26]. On Pluto, CO has an interesting and complex relationship with N<sub>2</sub> and CH<sub>4</sub> in certain geological regions across the surface, as observed by New Horizons.

The thermophysical and rheological properties of CO<sub>2</sub> and CO are measured through several previous experimental works, which are reviewed in brief here. Such an understanding of these primary C-bearing ices across the Solar System can give us insight into the geoscientific complexity of these simple volatiles.

A major step toward explaining the nature of these ices on various planetary surfaces and establishing their evolutionary origins requires accurate knowledge of their thermophysical and chemical properties. This review offers a primer on the current state of knowledge of CO<sub>2</sub> and CO ices, and furthermore highlights future, detailed laboratory work and further planetary mission objectives. We have organized our review of CO<sub>2</sub> and CO ices into the regions which they are situated on various icy satellites. We review the mineralogical and rheological properties of CO<sub>2</sub> and CO ices from (limited) experimental research, followed by the chemical aspect of spectroscopic observations of these ices.

We then review the geologic nature of CO<sub>2</sub> and CO ices from Jovian, Saturnian, Uranian, and Neptunian satellites, Pluto, and comets, including the possible origins of the ices, such as from subsurface oceans and UV irradiation. We conclude with a summary of our review and recommendations for future investigations.

## 2. Mineralogical and Rheological Properties

The satellites of the gas and ice giants and bodies of the Kuiper Belt harbor surface ice made of volatile molecules, clathrates, and complex hydrocarbons. Orbiter and fly-by images reveal complex geological structures across these satellites, where the materials are shaped by intricate physical processes. To understand the nature of these geologic variations on these icy surfaces requires knowledge of the mineralogical physics, such as the thermophysical and rheological properties of the ice. The rheology of ice is controlled by many factors, such as temperature, grain size, porosity, and stress, most of which are highly influenced by the impurities or the crystalline shape (e.g., hydrate cages vs. crystalline phases) [27,28]. While regolithic properties are determined through remote spectral observations of ground-based telescopes or mission data, the majority of these are estimates based upon Hapke modeling [29], which often relies on several assumptions regarding albedo effects, optical properties, compositions, and grain sizes and shapes—all parameters that are poorly constrained by these volatiles, often due to a lack of experimental data.

On the basis of an erosional view of the ices and how the CO<sub>2</sub> and CO ices can behave differently via sublimation or deposition, we can hypothesize that these ices would differ across these icy surfaces. The materials disaggregate from each other, causing collapse and slope retreat, resulting in smooth, undulating, low albedo plains of lag deposits, usually leaving H<sub>2</sub>O isolated on the top of localized summits and CO<sub>2</sub> within cold traps at lower elevations [30]. On Mars, the northern polar cap is shaped by ice sublimation and deposition [21], along with the distinctive pitting and outgassing geysers in the southern CO<sub>2</sub> pole [22,23,31]. However, on Pluto, CO is found in trace amounts in the atmosphere and condenses onto Sputnik Planitia or latitudinal regions with concentrations of N<sub>2</sub> or CH<sub>4</sub> [32,33].

While water ice is the main component across these surfaces, CO<sub>2</sub> and CO still have some interesting rheological information, which we briefly review here. Currently, most models rely on laboratory-derived empirical relationships, which are essential for the thermal modeling of the complex structures that are observed across the surfaces—such as faults and graben, geysers, impact craters, lineae, furrows, and possible cryovolcanic terrains [34]. These various endogenic and exogenic processes need an underlying understanding into the lithospheric nature of the ices for resurfacing and strains. The eruption of liquids through an icy crust can be complex due to the presence of contaminants, such as hydrates, which could vary its relative density. The presence of CO<sub>2</sub> or CO in such an icy mixture can therefore influence the density of the melt, buoyancy of the melt, and crystallization (including temperature and pressure conditions) of the matrix (see [28]). We briefly review the current state of low-temperature CO<sub>2</sub> and CO experimental research done with these ices, though unfortunately, there is a lack of CO-specific experimental research compared to CO<sub>2</sub>.

CO<sub>2</sub> has an amorphous solid phase at <30 K conditions and then transitions to a cubic phase [35]. Its triple point is located at 216.58 K (5.18 bar pressure). CO has two crystalline phases, the  $\alpha$ -CO phase (cubic) transitions to the  $\beta$ -CO (hexagonal) phase at ~61.6 K [36,37]. Under sufficient pressures ( $\mu$ bar), CO usually would sublime long before reaching 61.6 K. [38] have collected sublimation pressures of astrophysical ices, of which CO<sub>2</sub> and CO are listed here in Table 1. From those sublimation pressures, sublimation rates can be calculated (see [39]). Sublimation rates vary on these icy bodies (Figure 4), with Pluto and Triton at lower temperatures to allow CO to condense, although CO<sub>2</sub> is considered negligible at temperatures < 30 K due to the amorphous phase of CO<sub>2</sub> being unstable to solidify at planetary surfaces [4]. At conditions > 60 K, CO<sub>2</sub> becomes the more dominant volatile ice, and CO becomes unstable. Note that in a laboratory setting, growing

amorphous ice versus crystalline ice requires low deposition rates; indeed, the splitting of the  $\nu_2$  bending mode is a sign that some degree of crystallinity is present within pure  $\text{CO}_2$  ices [40].

**Table 1.** Sublimation pressures and temperatures of  $\text{CO}_2$  and  $\text{CO}$  ices. Values from [38] and references therein.

Species	Temperature (K)	Pressure (Bar)
$\text{CO}_2$	70	$1.00 \times 10^{-13}$
	80	$3.98 \times 10^{-11}$
	90	$6.31 \times 10^{-9}$
	100	$2.00 \times 10^{-7}$
$\text{CO}$	70	0.158
	80	0.631
	90	2.51
	100	6.31

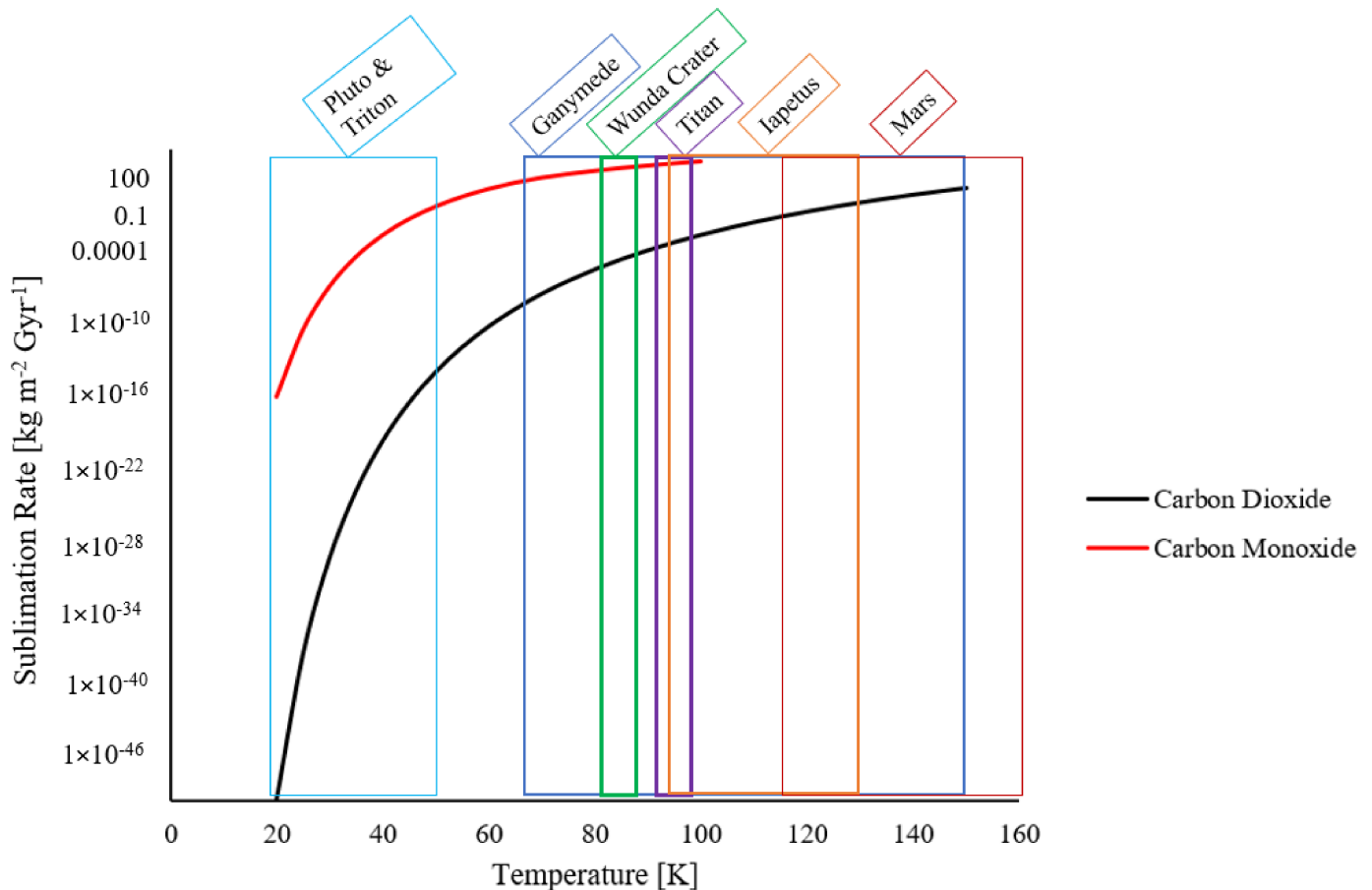


**Figure 4.** Sublimation rate curves for  $\text{CO}$  and  $\text{CO}_2$ . Colored bars represent the temperature ranges of different icy satellites and Mars. Note that  $\text{CO}_2$  is negligible at temperatures  $< 60$  K in terms of thick deposits, such that it is not a viable ice source at Pluto and Triton.

The thermal evolution of the ices, and on a macro scale, the evolution of the structural geologies on icy surfaces, depend greatly on the relative densities of phases. The density of ices can also influence how the subsurface ices can be buoyant in potential oceans or the density of grains for mass transport or erosional resistance [28]. From Table 2, the density of  $\text{CO}_2$  is  $\sim 1.4 \text{ g cm}^{-3}$ , increasing as temperature increases [41]. The pure  $\text{CO}$  densities

have not yet been experimentally researched in different thermal ranges, but pure CO is  $1.02 \text{ g cm}^{-3}$  at 30 K [42,43]. However, the density of CO in  $\text{N}_2$  has been measured (Table 3) [44]. It has been estimated that CO densities may be close to  $\text{N}_2$  ices for the purpose of Plutonian glaciation models [45].

**Table 2.** Density of  $\text{CO}_2$  ices at low temperatures as measured by Satorre et al. [41].

Species	Temperature (K)	Density ( $\text{g cm}^{-3}$ )
$\text{CO}_2$	10	1
	30	1.17
	40	1.25
	50	1.45
	70	1.48
	80	1.51

**Table 3.** Density of CO in  $\text{N}_2$  mixtures as determined by the molar ratio of CO within the mixture at a constant temperature of 14 K. Experimental values from Satorre et al. [44].

%CO	Density ( $\text{g cm}^{-3}$ )
10	0.94
20	0.87
30	0.87
50	0.89
70	0.92
90	0.95

The elastic properties of ice determine how much the ice crystal will compress given an external pressure. The ratio of the stress to the strain, regarding those compressional forces, defines Young's modulus.  $\text{CO}_2$  Young's modulus at 80 K is 13.12 GPa [46]. Ice  $\text{I}_h$  at that same temperature is  $\sim 0.1\text{--}0.5$  GPa [28].

Another thermodynamic property that could affect the crystallinity of  $\text{CO}_2$  and CO is sublimation energy, the heat required to change a solid phase constituent to the vaporous gas phase.  $\text{CO}_2$  has higher sublimation energies than CO by a factor of  $\geq 3$  (see [47]).  $\text{CO}_2$  at 80–90 K temperatures, the sublimation energy is 22.37 kJ/mol and then increases as the temperature increases. In contrast, CO at temperatures  $< 60$  K ranges from 6.3–7.9 kJ/mol (Table 4).

**Table 4.** Sublimation energy (E) of  $\text{CO}_2$  and CO as experimentally measured by Luna et al. [47].

Species	Temperature (K)	E ( $\text{kJ mol}^{-1}$ )
$\text{CO}_2$	91.5–92.5	29.3
	80–90	22.37
CO	33.5–34.5	6.3
	40–50	7.98
	54–61	7.6

In water ice containing  $\text{CO}_2$  and CO, crystallization times for amorphous water ice drops between 100–150 K, which is the average temperature range that may occur on Ganymede and Callisto [48]. From Schmitt et al. [48], an example of the crystallization time for water ice at 140 K (equatorial daytime temp on Ganymede) is  $\sim 1$  h. The depletion of the volatiles from a water ice lattice at that same temperature is a slightly longer time, as the crystallization process squeezes the  $\text{CO}_2$  or CO out of the water lattice [49]. The crystallization time increases to 700 h at 120 K, whereas it is on the order of  $2 \times 10^5$  years at 90 K. Therefore, small molecules will stay in the lattice in the polar regions for longer periods of time. However, in a volatile-rich equatorial region with more sunlight and therefore

increased temperatures, those small molecules may be driven out of the solid and form other condensing products or form transient atmospheres/exospheres [50].

The fact that CO<sub>2</sub> (and CO) persist on many of these surfaces despite their substantial vapor pressure at the temperatures of these bodies has largely been placed on the fact that these volatiles are either mixed or trapped with other species. In particular, the trapping of CO/CO<sub>2</sub> volatiles within clathrates has been suggested to play a major role [51]. CO<sub>2</sub> mixed with H<sub>2</sub>O ice could be in the form of a clathrate or other state that could occupy two different kinds of “sites” in a lattice. These “sites” are interstitial, where CO<sub>2</sub> is caught in-between two regularly spaced H<sub>2</sub>O molecules, or these can be substitutional, where CO<sub>2</sub> takes the place of a regular H<sub>2</sub>O molecule in the lattice [49,52]. Such arrangements in an H<sub>2</sub>O-CO<sub>2</sub> mixed ice can cause differences in the IR spectra, including and most diagnostically, the band positions, depending on if the CO molecules are interstitial or substitutional [49,53]. Clathrates in general have a peculiar thermodynamic behavior compared to crystalline water ice. The presence of guest gases within the water ice cage influences the molecular interactions, and therefore the stability and physical mechanics of the crystalline structure to be different. Clathrate hydrates with CO<sub>2</sub> (or N<sub>2</sub> or CH<sub>4</sub>) are generally less dense than the various high-pressure water ices [54], which may influence geologic structures overlying subsurface oceans, though more experimental research is warranted.

### 3. Chemical and Spectral Aspects

Solid CO<sub>2</sub> has also been detected in the interstellar medium (ISM) by the Spitzer Space Telescope and other telescopic observations [55,56]. Solid CO<sub>2</sub> is a major component of the icy mantle coating sub-micron-sized dust grains [57]. In the cold ISM, the oxidation of solid CO could lead to the formation of CO<sub>2</sub>, perhaps with a mixture of CO:O<sub>2</sub> ice [57,58]. O atoms needed may have been accreted in the grain, or resulted from dissociation of molecules, such as O<sub>2</sub> or H<sub>2</sub>O, by radiation (such as Ly $\alpha$ , stellar winds, cosmic rays) [59–61].

Both the experimental and model simulation of the processes occurring within the radiation tracks of ionizing radiation, as well as those instigated by UV photons, primarily result in the production of suprathreshold radicals and atoms, which are not in thermal equilibrium with their surrounding environment. Such species can surpass typical reaction barriers and lead to unusual chemical processes [58,62,63].

Lab studies have demonstrated that the irradiation of solid CO or mixtures thereof (with water or solid O<sub>2</sub>) can produce CO<sub>2</sub>, but CO<sub>2</sub>:CO ratios much smaller than those observed in the ISM [64–66]. On the other hand, CO<sub>2</sub> grains produced from CO + O reactions and CO radiolysis can (if heated) increase this ratio due to the higher volatility of CO [59]. Lab experiments demonstrate that radiolysis of H<sub>2</sub>O ice and C-rich substrates driven by charged particle irradiation can generate CO<sub>2</sub> [43,67–71]. The CO<sub>2</sub> produced by bombardment of ions and UV photons in simple ices effects such processing ranges, from ion sputtering, physical modification of the crystalline structure, and induction of non-thermal chemical reactions resulting in the refractory of organic residues [72–75]. In the temperature range of the Galilean satellites at 97–157 K, H<sub>2</sub>O and CO<sub>2</sub> can interact in a variety of ways, especially if the product of the plasma radiolysis is an H<sub>2</sub>O/CO<sub>2</sub> ice. For example, if an amorphous water ice containing CO<sub>2</sub> (or radiolysis products) is heated, volatile products (e.g., CO) produced by plasma bombardment will then be driven off by thermal cycling as the water ice recrystallizes at the higher temperatures, leaving refractory residual materials [48,61,73,76]. Irradiation of H<sub>2</sub>O/CO<sub>2</sub> ices will preserve the presence of CO<sub>2</sub> and CO above their normal sublimation temperatures [49]. Brucato et al. [77] observed that CO and CO<sub>2</sub> were still present up to 157 K, even though CO typically sublimates at 30 K and CO<sub>2</sub> sublimates at 72 K. Despite differences in the experimental results and parameters, all agree that the irradiative products of CO, CO<sub>3</sub>, and H<sub>2</sub>CO<sub>3</sub> (carbonic acid) are formed, and potentially O<sub>2</sub>, H<sub>2</sub>O<sub>2</sub>, and O<sub>3</sub>, which are observed at Europa (see Figure 5) [78]. Carbonic acid (H<sub>2</sub>CO<sub>3</sub>) has been suggested to be present on several icy surfaces, as it is a radiation product of H<sub>2</sub>O:CO<sub>2</sub> ices and potentially alongside formic acid (HCOOH) [61,79,80]. However, it has not been detected on comets and is unlikely to be on

cometary surfaces traveling through the inner solar system.  $\text{H}_2\text{CO}_3$  has a low sublimation temperature and thus would sublimate from the surface long before a comet reaches the inner solar system.

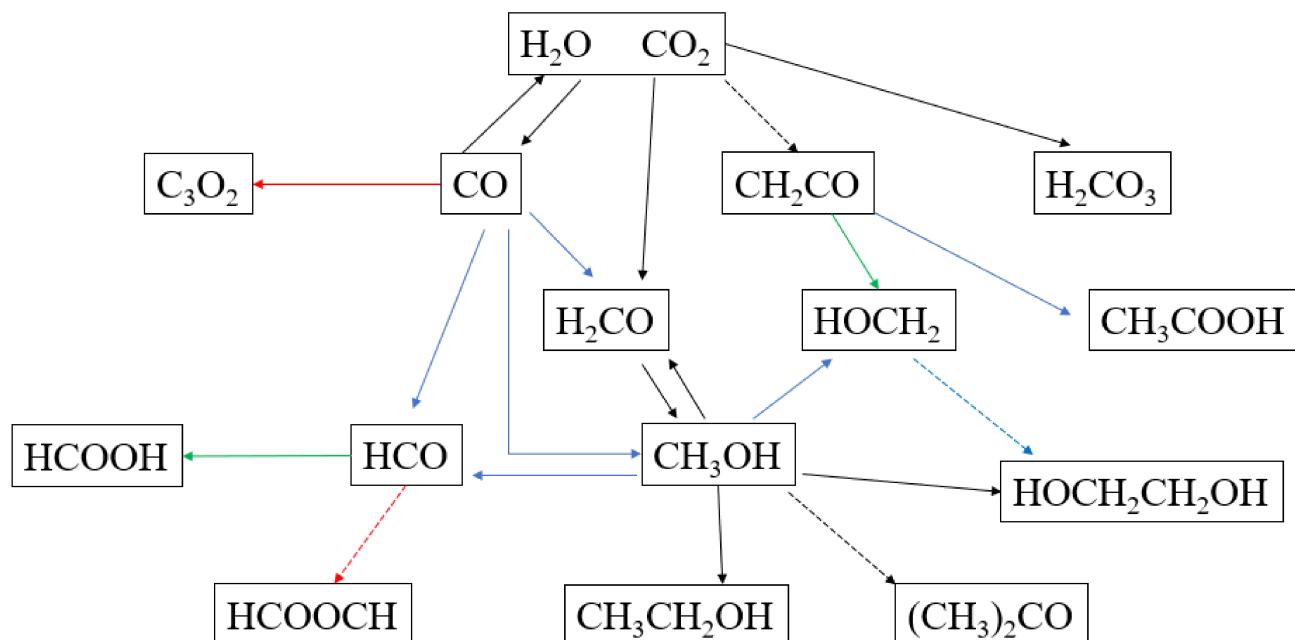


**Figure 5.** Potential reaction pathways (solid black lines) that occur in irradiated  $\text{H}_2\text{O}-\text{CO}_2$  ices, derived from laboratory experiments. Not all pathways are shown, and some pathways need to be re-evaluated by additional experimental research (dashed black lines). Figure adapted from [49]. Blue solid lines require the addition of  $\text{H}_2\text{O}$ ; red solid lines require the addition of  $\text{CO}$ ; green solid lines ( $\text{OH}$ ); red dashed lines ( $\text{HCO}$ ); and blue dashed lines ( $\text{HOCH}_2$ ). We note that although these species can be generated from  $\text{H}_2\text{O}$  and  $\text{CO}_2$  ices, other components present can also lead to, and influence, the distributions of these products (e.g.,  $\text{CH}_4$ ,  $\text{CH}_3\text{OH}$ ,  $\text{O}_2$ , etc.).

The Pioneer, Voyager, and Galileo missions paved the way for the understanding of the chemistry of the Jovian satellites [81]. The Galileo spacecraft obtained results from the solid-state imaging camera (SSI) and the NIMS instrument, operating in the range of  $0.7\text{--}5.2\ \mu\text{m}$  [82]. Further missions, such as Cassini and its Visual and Infrared Mapping Spectrometer (VIMS) and the New Horizons Linear Etalon Imaging Spectral Array (LEISA), have provided more information on the ices on Saturn and Pluto, respectively [83,84]. If we were to compare the spectra of Triton and Pluto (Figure 6), we see that the deeper  $\text{CO}_2$  spectral bands are very prominent in the Triton spectra, including a more major  $2.35\ \mu\text{m}$   $\text{CO}$  band depth than Pluto's.

It has been observed that the  $\text{CO}_2$  spectral profiles vary across the outer solar system and are certainly influenced by environmental conditions, such as temperature, which are still being investigated. Some hypotheses on the differences of spectral profiles include the following: (i) the mixing or entrapment of  $\text{CO}_2$  (or  $\text{CO}$ ) with  $\text{H}_2\text{O}$  and other volatiles (or organics) [3,85,86]; (ii)  $\text{CO}_2$  absorbed in minerals [87]; or (iii) clathrates [51].

Pure  $\text{CO}_2$  has a prominent spectral band at  $2340\ \text{cm}^{-1}$  ( $4.27\ \mu\text{m}$ ) [86,88]. From Table 5,  $\text{CO}_2$  shows a variety of other spectral bands if mixed with  $\text{H}_2\text{O}$  [89]. Pure  $\text{CO}$  also has several spectral bands in the near-IR [90]. On Callisto and Ganymede, the  $\text{CO}_2$  bands are centered at  $2348.5\text{--}2349\ \text{cm}^{-1}$  ( $4.258\text{--}4.257\ \mu\text{m}$ ) [91,92], while Iapetus and Phoebe have  $\text{CO}_2$  spectral bands at  $2347\ \text{cm}^{-1}$  ( $4.261\ \mu\text{m}$ ) [7,93]. A hypothesis on the down-shifting of the  $\text{CO}_2$  on Phoebe and Iapetus includes the  $\text{CO}_2$  being physisorbed in other host materials, such as clays [87].

**Table 5.** Prominent spectral bands in the IR wavelengths and respective vibrational modes.

Species	Mode	Band (cm <sup>-1</sup> )	Band (μm)
CO <sub>2</sub> <sup>a</sup>	$\nu_1$	1385	7.22 <sup>b</sup>
	$\nu_2$	660, 665	15.15, 15.04
	$\nu_3$	2340	4.274 <sup>c</sup>
	$2\nu_2 + \nu_3$	3592	2.784
	$\nu_1 + \nu_3$	3700	2.703
	$2\nu_3$	4685	2.134
	$4\nu_2 + \nu_3$	4832	2.070
	$\nu_1 + 2\nu_2 + \nu_3$	4960	2.016
	$2\nu_1 + \nu_3$	5083	1.967
	$\nu_1 + 4\nu_2 + \nu_3$	6214	1.609
$2\nu_1 + 2\nu_2 + \nu_3$	6341	1.577	
$3\nu_3$	6972	1.434	
CO <sup>d,e</sup>	$\nu + \nu^f$	4278.5	2.33
	$2\nu$	4250.9	2.35
	$2\nu$	4198.2	2.38
	$2\nu$	4158	2.4
	$2\nu$	4150.9	2.4
	$2\nu$	4054.8	2.46
	$\nu$	2139.4	4.67
	$\nu$	2112	4.73
	$\nu$	2091.7	4.78
	$\nu$	2088	4.78
$\nu$	2039.9	4.9	

<sup>a</sup> Values from Bernstein et al. [89] and Gerakines et al. [95]; <sup>b</sup> This band is forbidden by the selection rules, but can be weakly observed, particularly in mixtures of H<sub>2</sub>O:CO<sub>2</sub>; <sup>c</sup> Pure CO<sub>2</sub> spectral band; <sup>d</sup> Values from the Grenoble astroPhysic and planetOlogy Solid Spectroscopy and Thermodynamics (GHOSST) database by Schmitt et al. [90]; <sup>e</sup> Many of these peaks are due to the C isotopes; <sup>f</sup> This band is due to neighboring molecules that absorb the photon and split between the two species rather than one mode 2ν, which would be at a lower frequency due to anharmonicity.

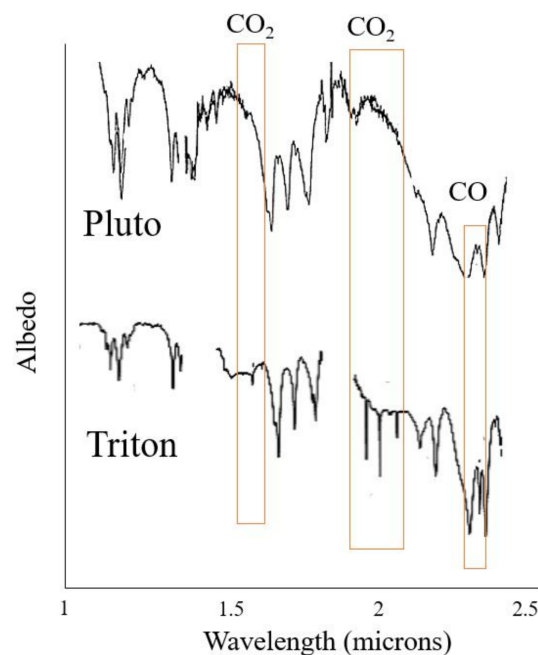


**Figure 6.** Telescopic spectra of Triton and Pluto with labeled CO<sub>2</sub> (1.65, 1.96 μm) and CO (2.35 μm) spectral bands. It should be noted that most of the remaining CO and CO<sub>2</sub> bands are spectrally interfered by more dominant CH<sub>4</sub> spectral bands [87]. (Pluto’s spectrum obtained from the UKIRT (adapted from [94]); Triton’s spectrum is averaged IRTF/SpeX (adapted from [11])).

## 4. Jupiter and Saturn

### 4.1. Ganymede

CO<sub>2</sub> ice is inferred to be present on the surface of Ganymede from Galileo NIMS (Near-Infrared Mapping Spectrometer) data [85,92] and is also detected by visible and UV absorption features [96,97]. Such absorption band signatures were distinct from those of pure solid or vaporous CO<sub>2</sub>, implying that the molecules are instead trapped or bound on the surface mixed with other species. This also provides a degree of thermal stability in that CO<sub>2</sub> is retained on surfaces that are otherwise at higher temperatures than the ~80 K at which CO<sub>2</sub> would otherwise be unstable due to sublimation [85]. The maximum surface temperature at Ganymede is ~152 K on the equator, but its poles do not exceed 80 K [98,99].

It is unlikely that there would be any amorphous CO<sub>2</sub> on any Jovian satellite since if CO<sub>2</sub> migrated to the poles from the equator of a satellite, it would condense on the surface above its amorphous-crystalline transition temperature. Upon reaching the poles, CO<sub>2</sub> condenses as crystalline CO<sub>2</sub> [49]. However, when subjected to plasma bombardment and irradiation, CO<sub>2</sub> produces other products, such as carbon suboxide (C<sub>3</sub>O<sub>2</sub>) and, in the presence of water, carbonic acid (H<sub>2</sub>CO<sub>3</sub>), on shorter timescales [100,101]. There also does not appear to be any leading or trailing hemisphere asymmetry in the distribution of CO<sub>2</sub>, nor do impact craters appear to be CO<sub>2</sub>-rich [92].

In the terrains where CO<sub>2</sub> is detected, it has been observed to be sufficiently large-grained [102]. Areas with finer-grained ice, like the polar regions of Ganymede, are not necessarily detectable, unlike Europa, for which small amounts of CO<sub>2</sub> have been detected in the finer-grained ices in its leading hemisphere [92]. On Ganymede, the bright sulci terrains contain less CO<sub>2</sub> than the dark terrains (Figure 7a), which are widely distributed  $\pm 60^\circ$  from the equator [92]. Distributions could be controlled by geological processes, plus effects from the Jovian (and thus Ganymede) magnetospheres, observing the following: (i) CO<sub>2</sub> not detected in polar regions; (ii) upper crust depleted of CO<sub>2</sub> (with the exception of Mir crater); (iii) deepest spectral bands of CO<sub>2</sub> found in darker, non-ice regions as detected by NIMS; (iv) dark crater ejects depleted in CO<sub>2</sub>; and (v) CO<sub>2</sub> exist in larger-grained equatorial regions [92].

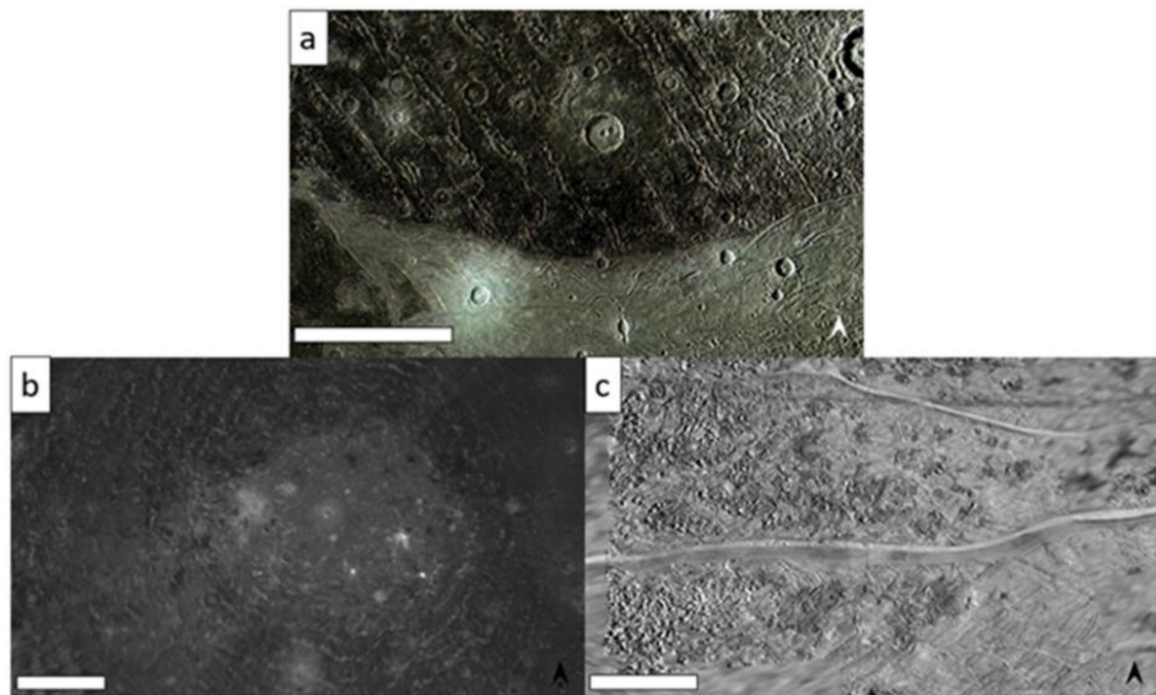


**Figure 7.** Examples of CO<sub>2</sub> features across some of the Galilean satellites. (a) Dark terrain and furrows on Ganymede (scale bar 250 km); (b) Callisto with brighter, fresher CO<sub>2</sub> deposits (scale bar 250 km); (c) Lineae features on Europa (scale bar 75 km).

Fresh impact craters on Ganymede do not contain any significant amounts of CO<sub>2</sub> or impurities, in contrast to Callisto [103]. Such a depletion of CO<sub>2</sub> in crater ejects implies that the interior of Ganymede has become depleted in CO<sub>2</sub>. The CO<sub>2</sub> lost from the interior is probably due to Ganymede's differentiation and tectonic history. It is also possible that the CO<sub>2</sub> was originally endogenous as a clathrate solution with the ice, depending on the temperature and pressure conditions, and was either absorbed into the non-ice material or as inclusions [92].

#### 4.2. Callisto

CO<sub>2</sub> and SO<sub>2</sub> have been observed on the surface of Callisto by the Galileo NIMS spectra [104]. CO<sub>2</sub> has varying concentrations except at higher latitudes, which may be attributed to water ice frost [85], implying more mobile and transient molecules of the frost. The CO<sub>2</sub> concentration on the trailing hemisphere has a longitudinal distribution largely consistent with a sinusoid centered on the equator near 270° longitude [104], suggesting exogenic effects related to Jupiter's magnetic field. Exogenic and endogenous mechanisms exist to explain the nature of CO<sub>2</sub> distributions. Such distributions suggest it originated from either in-falling CO<sub>2</sub>-rich material, surface chemistry, or exposure of subsurface deposits [104].

CO<sub>2</sub> appears to be more associated with enriched craters compared to the surrounding dark material (Figure 7b), suggesting impact processes that may also affect the distribution [103,104]. CO<sub>2</sub> could also originate from impact-related events, such as comets [105]. Low CO<sub>2</sub> in bolides and high concentrations in others would explain the CO<sub>2</sub>-poor and CO<sub>2</sub>-rich fresh impact craters in Burr and Tornarsuk craters, respectively [104]. Impact-related and/or in situ chemistry includes radiolysis as a means to produce CO<sub>2</sub> in the trailing hemisphere surface material and the chemistry of precursor materials subjected to high-velocity impacts.

For the trailing hemisphere, this region involves the effects of Jupiter's magnetic field, including the following: (i) implantation of magnetospheric bounded dust grains containing CO<sub>2</sub>; (ii) sputtering effects in an accumulation of CO<sub>2</sub>-bearing dark material; (iii) in situ radiolysis; and (iv) alteration of host material.

Callisto may also have an internal reservoir where strong surface CO<sub>2</sub> signatures are maintained while CO<sub>2</sub> is lost through a thin exosphere [106]. Such a subsurface CO<sub>2</sub> reservoir can be exposed by cratering. Variable CO<sub>2</sub> concentrations in ice-rich impact craters would reflect a subsurface inhomogeneity in CO<sub>2</sub> abundance. A CO<sub>2</sub> subsurface may be able to host CO<sub>2</sub> clathrates [107] and contain up to 0.01% of trapped molecules (including possibly CO) if double-caged [108]. Loss of CO<sub>2</sub> from ice on the surface could explain why the freshest craters are enriched in CO<sub>2</sub>.

#### 4.3. Europa

The formation of Europa assumes an origin in the Jovian sub nebula from material comparable to that of carbonaceous chondrites [109,110]. Assuming only CO<sub>2</sub> is derived from the leaching of this material, it is argued that the subsurface oceanic concentrations could be in the range of ~0.02–1.23% by number CO<sub>2</sub> [109]. If it erupted to the surface, solid CO<sub>2</sub> could be expected within the ice shell makeup. However, Galileo NIMS observations indicate an abundance of CO<sub>2</sub> of 0.08% [111], although NIMS data only represents the approximate uppermost millimeter of the surface, and (consequently), the most radiation-processed surface materials [112,113]. Therefore, NIMS may represent a lower limit of CO<sub>2</sub> concentration in the ice shell. CO<sub>2</sub>, when exposed to high-energy ions and electrons, evolves into CO and O, among other products [63,80]. Solid O<sub>2</sub> is not stable near the surface of Europa [79], although it is considered to be a radiation product. CO is highly volatile and would escape into the atmosphere and be ionized away by Jupiter's magnetic field. A tenuous CO atmosphere may exist on Europa, but no carbon lines of such a compound were seen in the collected spectra by Hall et al. [114]. CO<sub>2</sub> is also found on Europa's trailing anti-Jovian hemisphere [115], where carbon supposedly originates from

micrometeorites within 1.5–12 g/s (at the Galilean satellites), at ~3 g/s for Europa [112]. This is associated with darker hydrate materials and with non-ice materials comparable to Callisto and Ganymede [92]. The hydrate distribution in the chaos and linea geologic structures (Figure 7c) may be associated with European interior dynamics [116,117].

The Galileo NIMS and the Hubble Space Telescope, along with lab experiment results, indicate the production of oxidant compounds ( $\text{H}_2\text{O}_2$ ,  $\text{CO}_2$ ,  $\text{SO}_2$ , etc.) is a consequence of radiolytic chemistry [112,118]. Once created, these products may be entrained deeper into the ice shell through resurfacing processes like tectonism or impacts. The temperature and pressure within the hydrosphere are also conditional for the formation of clathrate compounds like  $\text{CO}_2$  clathrates [119]. Since  $\text{CO}_2$  is strongly associated with the endogenous dark (typically hydrated) regions, this may indicate a  $\text{CO}_2$ -rich ocean that is a potential environment for autotrophic organisms that may thrive at rock-ocean interfaces [115,120].

#### 4.4. Io

$\text{SO}_2$ ,  $\text{H}_2\text{S}$ ,  $\text{H}_2\text{O}$ , and  $\text{CO}_2$  have been identified (even tentatively) on Io through infrared spectroscopic techniques [121–123].

If  $\text{CO}_2$  exists on Io, it might be present in the form of an aerosol or thin surface frost over localized spots [124].  $\text{CO}_2$  may also be intimately mixed with  $\text{SO}_2$ -rich ices and frosts [124,125].  $\text{CO}_2$  is expected to form at temperatures typical of colder spots on Io [123]. However, these  $\text{CO}_2$  cold spots are not expected to be stable at temps above 100 K, while daytime temps on Io can reach 130 K, and  $\text{CO}_2$  leads a rather nomadic, transient existence on the surface.

#### 4.5. Saturnian System

$\text{CO}_2$  deposits in the Jupiter-Saturn systems are associated with low albedo and organic-rich regions [51,115,126]. Aside from  $\text{CO}_2$  ice associated with fresher impact craters on Callisto [103] and  $\text{CO}_2$  detected in plumes emanating from Enceladus [127], there appears to be no clear correlation of  $\text{CO}_2$  with geologic features. However, spatial correlation of  $\text{CO}_2$  and  $\text{H}_2\text{O}$  ices support active UV photolysis and radiolysis mechanisms [128,129].

Europa, Callisto, and Dione are all embedded within their host planet's magnetospheres,  $\text{CO}_2$  on trailing hemispheres, all relating to particle photolysis mechanisms. Ganymede is also embedded, but its intrinsic magnetic field deflects charged particles, which may explain why there is no clear asymmetry of  $\text{CO}_2$ . Hyperion (chaotic rotation) and Phoebe (non-synchronous rotation) also do not display hemispherical asymmetries. Iapetus does have obvious hemispherical asymmetries in its  $\text{CO}_2$  abundance, but it has been observed that its low albedo is in the leading hemisphere, while  $\text{H}_2\text{O}$  is in the trailing hemisphere [130].

#### 4.6. Enceladus

Accumulations of solid  $\text{CO}_2$  were identified on the surface of Enceladus, mostly concentrated at the southern pole (Figure 8a) [5].  $\text{CO}_2$  ice sublimates in Enceladean conditions, thus these deposits must be sustained by some mechanism, such as the transport of  $\text{CO}_2$  from the subsurface ocean [5,131,132]. The  $\text{CO}_2$  deposits within the polar cold traps may persist for up to 6 years before subliming [5].

At the southern pole, Enceladus houses the famous “tiger stripes”—fissure-like thermally-dynamic features [132], where  $\text{CO}_2$  deposits are on the surface and in the gaseous phase within the subsurface ocean, as observed in the plumes, as imaged by Cassini in 2004 [5,131]. In fact, most of the highest concentrations of  $\text{CO}_2$  were found in the regions between the tiger stripes [132]; however, the deposition cannot come directly from the plumes, otherwise water would dominate the signal.  $\text{CO}_2$  emerges from the subsurface ocean in the following two main ways: (i) seeping, in which pockets of pure  $\text{CO}_2$  ice are created; or (ii) blowouts, which emit both  $\text{CO}_2$  gas and aerosols [5].  $\text{CO}_2$  clathrates are also potentially deposited within an average of 17 m of the vents [5]. Combe et al. [132] were able to identify both pure and mixed  $\text{CO}_2$  ice, again with the highest levels between the

main active faults of the south polar region (notably where the temperature is the lowest). This implies how CO<sub>2</sub> frosts accumulate between the tiger stripes, since other regions would vaporize the CO<sub>2</sub>.

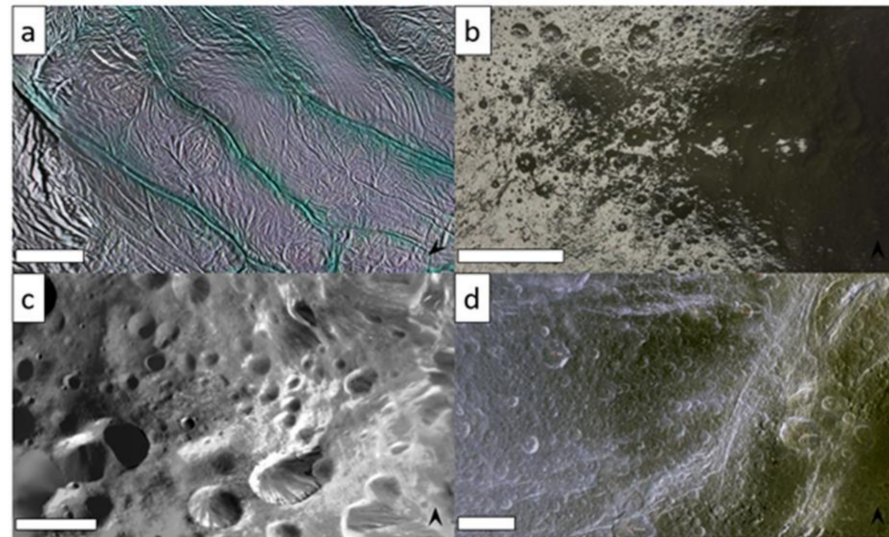


**Figure 8.** Examples of CO<sub>2</sub>-specific regions on Saturnian satellites as imaged by Cassini. (a) Tiger stripe southern pole on Enceladus (scale bar 25 km); (b) the darker leading hemisphere of Iapetus transitioning to the lighter albedo trailing hemisphere (scale bar 250 km); (c) cratered surface of Phoebe (scale bar 25 km); (d) Darker terrain on Dione (scale bar 100 km).

#### 4.7. Hyperion and Iapetus

The 134.8 km-diameter satellite Hyperion is mostly composed of water ice, though CO<sub>2</sub> has also been observed, possibly mixed with the H<sub>2</sub>O ice [51] or as a clathrate [133]. The low density of the surface has collapsed pockets of low-albedo material, indicative of minor irradiative carbon-bearing ices [51]. Unlike Iapetus, Hyperion's CO<sub>2</sub> seems to be distributed across high-, low-, and mid-albedo materials.

Iapetus has the most extreme albedo contrasted surface in the Saturnian system (Figure 8b), where the leading hemisphere and equatorial region have a low albedo of 2–6%, and the trailing hemisphere and poles have a 10× greater reflectance of H<sub>2</sub>O ice [7]. Pure CO<sub>2</sub> ice is unstable under Iapetus' conditions [93], and instead pure CO<sub>2</sub> is generated through the photolysis of O and C in mixtures with other compounds, including H<sub>2</sub>O [128]. The CO<sub>2</sub> then moves ballistically around the atmosphere until it reaches the poles (with some atmospheric escaping effects), where it is stabilized by the cold temperatures (~130 K) and sequestered for up to 15 years [93,128]. Iapetus' obliquity, interestingly enough, causes the CO<sub>2</sub> to switch hemispheres [128], estimating that ~12% of the CO<sub>2</sub> cap is lost during a complete yearly cycle.

The CO<sub>2</sub> formed on Iapetus is also photolyzed by UV radiation and cosmic ray mechanisms [128,134]. Since UV radiation and cosmic rays are the potential culprits for the irradiation mechanisms on CO<sub>2</sub>, the low-albedo regions may contain C-bearing molecular species, such as CH<sub>4</sub>. From experimental work, radiation of water-covered graphene (or graphene oxides) produces CO<sub>2</sub> during these processes, including UV and various radiation sources [70].

From the Cassini VIMS data, the H<sub>2</sub>O ice mixes with the CO<sub>2</sub> and the CO<sub>2</sub> band shifts [7]. Both Iapetus and Phoebe display shifted CO<sub>2</sub> bands, indicating these surfaces are H<sub>2</sub>O ice poor, but not necessarily ice-free [7].

#### 4.8. Phoebe and Dione

On Phoebe, the Cassini VIMS instrument shows spectra indistinguishable from pure CO<sub>2</sub> ice or from the Type II clathrate (where the ratio of water and another molecule is

larger than Type I at 17:1; [51,135], where the central band of pure CO<sub>2</sub> is at ~4.27 μm (2340 cm<sup>-1</sup>) [51]. However, it has been observed that the CO<sub>2</sub> bands are correlated in some places with the H<sub>2</sub>O spectral bands and are more spatially variable [51], suggesting that the surface may also include liquid or gaseous CO<sub>2</sub> [7].

Phoebe is comparatively far from Saturn (~0.086 AU) (Figure 8c), so the destruction or transformation of CO<sub>2</sub> ice on the surface is predominantly due to cosmic rays and solar UV, as opposed to the magnetosphere [51]. Interestingly, Phoebe has a sufficiently strong CO<sub>2</sub> band to reveal its <sup>13</sup>C/<sup>12</sup>C ratio, which is unusually high (by nearly 4.7 times) than the other Saturnian satellites (see [93]).

For Dione, the surface is almost entirely high-albedo H<sub>2</sub>O ice, but a weak spectral band of CO<sub>2</sub> has been measured in the lower-albedo trailing hemisphere (Figure 8d) [51].

#### 4.9. Titan

Titan's methane-rich, aerosol-filled atmosphere complicates the identification of surface compositions in the near-IR [83], though CO<sub>2</sub> has been identified in the atmosphere through ground-based telescopes and VIMS onboard the Cassini spacecraft, including CO<sub>2</sub> detected in Titan's nightside atmosphere at 4.30 μm [83].

### 5. Uranus and Neptune

Uranus (~19.8 AU) and Neptune (~30.1 AU) have an enrichment in carbon. The density of solids in the outer protosolar nebula is too low to fully explain these icy giant formations. Ali-Dib et al. [136] suggest that this can be explained if Uranus and Neptune originally formed at the CO ice line (at a maximum distance of 28 AU), possibly due to the diffusion and redistribution of vapors, and that these planets are in N<sub>2</sub>-poor (or N<sub>2</sub>-depleted) gas environments. Calculating the composition and properties of the CO ice line, including turbulent drag, sublimation, gas diffusion, and condensation for vapors, gives this ice line a natural depletion in N<sub>2</sub> vapor [136].

The surfaces of the Uranian satellites are characterized by a mixture of H<sub>2</sub>O ice and a dark, low-albedo constituent, potentially of C-rich material, along with CO<sub>2</sub> ice [26]. At the heliocentric distance of the Uranian system, native CO<sub>2</sub> should be removed on timescales shorter than the age of the Solar System (see [136]). Therefore, the detected CO<sub>2</sub> (through the use of spectrometers, such as the SpeX spectrograph at NASA's Infrared Telescope Facility—IRTF [26]; on these moons may be actively produced. Analogous to the irradiative processes on the Jovian and Saturnian moons, charged particles caught in Uranus' magnetic field bombard the surfaces, driving a radiolytic CO<sub>2</sub> production cycle.

CO<sub>2</sub> ices, through recent near-IR observations, have been detected over both hemispheres of most Uranian satellites, with the strongest CO<sub>2</sub> in the trailing hemispheres closest to Uranus, as compared to the H<sub>2</sub>O in the leading hemispheres [137]. However, there is no detection of CO<sub>2</sub> on Miranda, and the CO<sub>2</sub> on Oberon is still debatable [137,138].

The potential sources of CO<sub>2</sub> on the surfaces of these satellites have multiple possible origins, such as the following: (i) accretion with primordial materials through impacting or tectonically exposed or emplaned by cryovolcanism [26]; (ii) exospheric delivery of non-native CO<sub>2</sub> molecules sourced from different sources through or outside the Solar System (i.e., interstellar dust); (iii) re-deposition of sublimated native CO<sub>2</sub> in cold traps; and (iv) non-native O<sub>2</sub> synthesized by electron, ion, and UV irradiation. Sublimation of CO<sub>2</sub> driven by subsolar heating is unlikely to influence the observed distribution given that this mechanism should operate evenly in both hemispheres, leading to the homogenizing of the CO<sub>2</sub> distribution. Similarly, UV photolysis should also operate evenly and is also an unlikely driver of hemispherical asymmetries [26].

CO<sub>2</sub> is detected on Umbriel, Ariel, and perhaps Oberon and Titania [138]. However, only Umbriel has a prominent bright deposit of CO<sub>2</sub>. Why does only Umbriel have a large deposit of CO<sub>2</sub>? The following three possibilities arise: (i) solid, locally concentrated CO<sub>2</sub> ice deposits not currently present on the surface of the other satellites, (ii) or not

yet observed (due to limited, low-resolution data from Voyager 2) or (iii) obscured by sublimation lag by carbonaceous material.

Umbriel has a prominent high-albedo annulus-shaped feature at the pole within the 131 km-diameter impact crater Wunda [39]. Considering sublimation and atmospheric escape on Umbriel, CO<sub>2</sub> ice migrates to low latitudes on geologically short (100–1000 s of years) timescales. Therefore, the Wunda crater serves as a local cold trap for CO<sub>2</sub> (Figure 9a). The high albedo combined with the thermal inertia of CO<sub>2</sub> relative to the regolith allows deposits of CO<sub>2</sub> at >15 m thick to be stable over the age of the Solar System [39]. There are, however, a few later native hypotheses for the CO<sub>2</sub> deposit in the Wunda crater. Cryovolcanism has been suggested as a possible source in addition to radiolytic production [26]. Extrusive CO<sub>2</sub> would be more plausible if instead the homogenous dark surface was representative of the upper crust, which would allow endogenous activity superposed on the dark surface to be relatively ancient [39]. CO<sub>2</sub> is also suggested to be excavated by impacts, like Callisto [103]. However, larger craters on Umbriel larger than Wunda do not contain similarly bright deposits, making this an unlikely direct excavation of CO<sub>2</sub> [39].

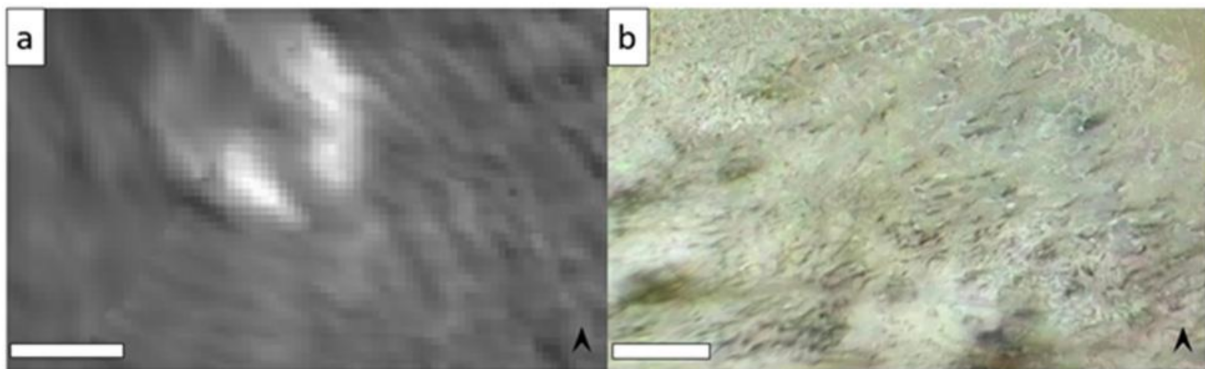


**Figure 9.** Voyager 2 images of CO<sub>2</sub> features on Uranian and Neptunian satellites. (a) Wunda crater CO<sub>2</sub> ice deposit (scale bar 75 km); (b) N<sub>2</sub> geysers with potential CO or CO<sub>2</sub> ice interactions at the southern pole of Triton (scale bar 250 km).

Ariel has been observed to have a partially young surface with resurfacing structures [139,140], perhaps by tidal heating. It is possible that older CO<sub>2</sub> ice deposits could be buried and resurfaced. While there are no extreme detections of CO<sub>2</sub> spectral signatures on Oberon [138], Cartwright et al. [26] argues for weak detection and statistically possible CO<sub>2</sub> deposits that may be small, localized cold traps under the resolution of the Voyager 2 flyby images. Weak detection may also be the result of Oberon's distance from Uranus. Oberon spends part of its orbit outside Uranus' magnetic field, making radiolytic production weak [39]. CO<sub>2</sub> ice is not expected to deposit on Miranda due to atmospheric escape, where Miranda's escape velocity of 193 m/s is far less than the other four satellites. Due to this circumstance, CO<sub>2</sub> is rapidly lost to space, with ~50% of sublimated molecules escaping.

There is a possibility that Ariel, Titania, and even Oberon have deposits, but these may be small (or buried), plus the fact that the current USGS maps of these satellites do not cover the entirety of these moons' surfaces due to the limiting images from Voyager 2. It is not surprising that Umbriel is the only satellite with fuller coverage centered on the trailing hemisphere [39].

Onward to the Neptune system, Triton has been observed to have both CO<sub>2</sub> and CO ices in the near-IR from the 3.9-m UK Infrared Telescope on Mauna Kea and the IRTF SpeX instrument [11,141,142]. While neither CO<sub>2</sub> nor CO gases have been seen by the Voyager 2 data, the presence of these ices are likely frozen in solid matrices of N<sub>2</sub> and CH<sub>4</sub> solids. The CO on Triton exhibits longitudinal variation, whereas the absorptions by H<sub>2</sub>O and CO<sub>2</sub> ices show a more uniform spatial distribution [143].

A major question is whether the CO molecules are diluted in N<sub>2</sub> ice or if the CO exists separately as a pure ice [144]. It is not surprising, however, for CO and N<sub>2</sub> mix as the compounds have similar volatility and are fully miscible in one another, in both liquids and solids. The two species could separate through a solid-state distillation process [144]. While the geysers on Triton are dominantly N<sub>2</sub> outgassing, CO ices could still potentially play a role in the structure and sublimation nature of the geysers (Figure 9b).

## 6. Pluto

Ices existing on Pluto include the volatile cryogenic CO, CH<sub>4</sub>, and N<sub>2</sub>, with H<sub>2</sub>O and complex organic materials [33]. A variety of processes modify its surface, from geologic to seasonal timescales. CO ices are easily mobilized at the low temperatures of Pluto's surface (~40 K) [33]. Pluto's CO, N<sub>2</sub>, and CH<sub>4</sub> ices are all volatile at Pluto's surface temperatures and support Pluto's atmosphere via vapor pressure equilibrium and seasonal cycle activity [33,145]. All of these ices are also soluble in one another to some degree, similar to ices on Triton [37,146].

CO never forms pure deposits on Pluto. Although CO is almost as volatile as N<sub>2</sub>, it is also found in trace amounts in the Plutonian atmosphere (thus requiring low temperatures to condense) as a consequence of Raoult's Law, controlling the vapor pressure equilibrium [32]. Therefore, for CO to be in some surficial solid form to condense and deposit, it would require it to be either in a mixture with N<sub>2</sub> or CH<sub>4</sub>.

The strongest CO spectral signatures (Figure 10a), as observed by the LEISA instrument onboard the NASA New Horizons mission, are found in the central and southern portions of Sputnik Planitia, along with the dominant N<sub>2</sub> spectral signatures. Sputnik Planitia having these two dominant volatiles leads to hypotheses on the densities of CO and N<sub>2</sub> ices and what role they may play in the convective nature of the basin's large icy cells and glaciation processes (Figure 10c) [32,45,147,148]. CO-CH<sub>4</sub> mixtures are mainly in the 40°–60° latitude band (Figure 10b) [84], mainly found in crater floors, southern Venera Terra, southwest Venera Terra, and eastern Hayabusa Terra.

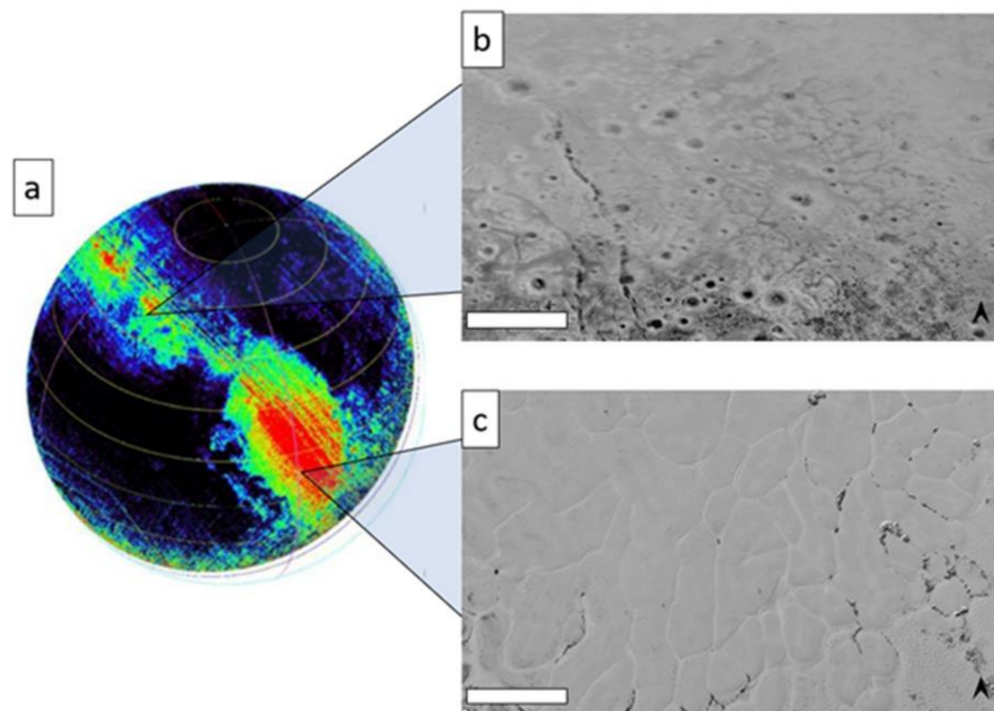


**Figure 10.** (a) CO concentrations on Pluto as observed by the LEISA instrument onboard the New Horizons spacecraft (see [84] on color scale and spectral measurements); (b) Venera Terra CO-CH<sub>4</sub> dominated region (scale bar 100 km); (c) central Sputnik Planitia basin with CO-N<sub>2</sub> ices (scale bar 75 km).

All of these combinations of a latitudinal trend or localized concentrations point towards a differentiation or separation process of CO occurring during the N<sub>2</sub>-rich to CH<sub>4</sub>-rich ice transition driven by N<sub>2</sub> sublimation [33].

## 7. Comets

While most comets are considered H<sub>2</sub>O-dominant, some comets have an abundance of carbon-bearing parent molecules of CO and CO<sub>2</sub>, such as comet Kohoutek (1973f) and comet West (1975n) (Ip 1983). CO gaseous emissions were detected at millimeter wavelengths in comet 29P/Schwassmann–Wachmann 1 at ~6 AU [149]. Thereafter, CO was detected in C/1995 O1 (Hale-Bopp) over 6–6.8 AU and in 2060 Chiron at 8.5 AU and 67P/Churyumov–Gerasimenko (see references in [149,150]). The CO production rates were high enough that CO outgassing was assumed to be the main component of activity for these comets. From Ip [151], addition of CO and/or CO<sub>2</sub> molecules (~30% in water) in a medium-bright comet are dissociated outside of the coma collision zone without depositing the excess kinetic energy to the neutral atmosphere, namely, due to the photodissociation length scales of these volatiles are a factor of 10–30 larger than H<sub>2</sub>O molecules. However, if the gas production rate is controlled by CO or CO<sub>2</sub>, the coma collision zone can be increased by a factor of 7, allowing the photochemical heating due to CO dissociation to be more effective in outbursting [151–153].

The gaseous emissions of CO<sup>+</sup> (and other volatiles such as CN and OH) are also observed in distantly active comets [154]. However, these cannot drive the activity due to their production through ionization or dissociation of other molecules in the coma and do not exist in the nucleus [149]. CO is difficult to photo-ionize beyond 5 AU, so detecting CO<sup>+</sup> implies either large amounts of CO being released in the coma or transient ionization mechanisms.

The European Space Agency's (ESA) Rosetta mission became the first spacecraft to follow a comet (Comet 67P/Churyumov–Gerasimenko) along its path, providing interesting information on the distribution and levels of production of H<sub>2</sub>O, CO<sub>2</sub>, and CO in the coma at 2.5–2.9 AU using its VIRTIS (Visible and Infrared Thermal Imaging Spectrometer) instrument [1,155–157]. Bockelée-Morvan et al. [155] suggested that CO<sub>2</sub> sublimates below the water ice diurnal skin depth (<1 cm) because CO<sub>2</sub> has been observed in both illuminated and non-illuminated regions of the coma, with outgassing mostly from the Northern and Southern hemispheres of Comet 67P. However, it should be noted that these observations are for a specific time (specifically, the Northern hemisphere summer) and are not representative of the whole nucleus. Fink et al. [158] proposed that the Northern hemisphere is depleted in CO<sub>2</sub>. The non-detection of CO<sub>2</sub> in the Northern hemisphere was measured before the May 2015 equinox using data from the RTOF (Reflectron Time-of-Flight) instrument, even though the surface temperatures (~200 K) were well above the sublimation temperature of CO<sub>2</sub>, suggesting an insulating layer of dust and water was transported from the Southern hemisphere [157], though CO<sub>2</sub> was detected in both hemispheres seasonally using the DFMS (Double-Focusing Mass Spectrometer) instrument [150]. From the ROSINA (Rosetta Orbiter Spectrometer for Ion and Neutral Analysis) instrument, high CO<sub>2</sub>/H<sub>2</sub>O ratios were observed on the southern side of the larger lobe, though mainly due to lower H<sub>2</sub>O concentrations [159]. Läuter et al. [159] observed that CO<sub>2</sub> was released from both coma hemispheres, but the production rate varied with heliocentric distance, though H<sub>2</sub>O was the most varied due to its higher sublimation temperature. With distance and changing illumination conditions, this led to low CO<sub>2</sub>/H<sub>2</sub>O in the Northern hemisphere inbound up to the equinox and a higher CO<sub>2</sub>/H<sub>2</sub>O in the Southern hemisphere. In terms of the cometary nucleus, which is much more difficult to discern, CO<sub>2</sub> has been seasonally detected on the surface of 67 P, attributed to CO<sub>2</sub> frost [156]. However, cometary comas are complex, and thus the reasoning for differential lobe composition for CO<sub>2</sub> and hemispherical asymmetry is inconclusive. These ratios do not reflect relative production over the entirety of the cometary body.

With the beginning of cometary measurements made by the Rosetta mission, future cometary missions (whether sample return, impactor sampling, or rendezvous) can improve our understanding of the origins and cycles of CO<sub>2</sub> and CO on these primitive icy bodies.

## 8. Summary

As we have noted in this geoscientific review, the thermodynamic and chemical properties of CO<sub>2</sub> and CO ices remain mostly as theoretical estimates in extreme conditions (e.g., subsurface oceans or extremely low temperatures and pressures) and we note that not only more experimental measurements are needed, but also more images from spacecraft are needed, especially those of the Uranian satellites and Triton. Further experimental work on CO<sub>2</sub> and CO can include further studies on thermal conductivity and expansivity, density of pure versus volatile mixtures, and diffusion creep. Our knowledge of the surface compositions and regional or localized variations of CO<sub>2</sub> and CO across these icy bodies has greatly improved our understanding of spectral behaviors, but it is the complexity and diversity of the emplacement mechanisms of CO<sub>2</sub> and CO ices that we must peer through to understand the properties of these ice phases. We have found that the CO<sub>2</sub> distribution varies across the outer Solar System, with various asymmetries in the Jovian and Saturnian systems, though Dione is supposedly the only Saturnian moon with a trailing hemisphere-dominant CO<sub>2</sub> signature. On Uranus, the CO<sub>2</sub> distribution is dominantly in the trailing hemisphere, with the strongest signatures being closest to Uranus. Their physical and chemical parameters, such as density and sublimation pressures, are key to modeling the endogenous and exogenous processes and understanding the variations of collected spectra from ground-based telescopes or spacecraft missions. Future planetary missions would benefit from an impact penetrator probe or sampling measurements of CO/CO<sub>2</sub> dominant hemispheres on the icy satellites, along with additional spectral observations in the near-infrared. The Uranian satellites would greatly benefit from a specific mission to determine the nature and distribution of these ices, especially verifying the presence of CO<sub>2</sub> ices across the satellites. While CO<sub>2</sub> and CO ices are not as widespread as other ices, such as water ice or methane, these volatiles are still worthy of geoscientific exploration in the outer Solar System. Understanding CO<sub>2</sub> and CO through additional experiments or mission observations (whether remote or sampling) can provide further insight into the complexity of CO<sub>2</sub> and CO origins across the Solar System, and how these compounds interact with volatiles in chemically, energetically, and geologically varying environments. Such characteristics of CO<sub>2</sub> and CO can enhance models regarding irradiative products, magnetic field and volatile interactions, and ocean dynamics.

**Author Contributions:** Conceptualization, C.A.; resources, H.M. and C.B.; writing—original draft preparation, C.A.; review and editing, C.A., H.M., C.B. All authors have read and agreed to the published version of the manuscript.

**Funding:** C.A. research was supported by an appointment to the NASA Postdoctoral Program at NASA Goddard Space Flight Center, administered by Universities Space Research Association under contract with NASA.

**Data Availability Statement:** This research does not report any data.

**Acknowledgments:** The authors wish to thank the Java Mission-planning and Analysis for Remote Sensing (JMARS) for the mapping capabilities to create the planetary surface figures.

**Conflicts of Interest:** The authors declare no conflict of interest.

## References

1. Bockelée-Morvan, D.; Biver, N. The composition of cometary ices. *Philos. Trans. R. Soc. A Math. Phys. Eng. Sci.* **2017**, *375*, 20160252. [[CrossRef](#)] [[PubMed](#)]
2. Schorghofer, N.; Williams, J.P.; Martinez-Camacho, J.; Paige, D.A.; Siegler, M.A. Carbon dioxide cold traps on the moon. *Geophys. Res. Lett.* **2021**, *48*, e2021GL095533. [[CrossRef](#)]
3. Chaban, G.M.; Bernstein, M.; Cruikshank, D.P. Carbon dioxide on planetary bodies: Theoretical and experimental studies of molecular complexes. *Icarus* **2007**, *187*, 592–599. [[CrossRef](#)]

4. Escribano, R.M.; Caro, G.M.M.; Cruz-Diaz, G.A.; Rodríguez-Lazcano, Y.; Maté, B. Crystallization of CO<sub>2</sub> ice and the absence of amorphous CO<sub>2</sub> ice in space. *Proc. Natl. Acad. Sci. USA* **2013**, *110*, 12899–12904. [[CrossRef](#)] [[PubMed](#)]
5. Matson, D.L.; Davies, A.G.; Johnson, T.V.; Combe, J.P.; McCord, T.B.; Radebaugh, J.; Singh, S. Enceladus' near-surface CO<sub>2</sub> gas pockets and surface frost deposits. *Icarus* **2018**, *302*, 18–26. [[CrossRef](#)]
6. James, P.B.; Kieffer, H.H.; Paige, D.A. The seasonal cycle of carbon dioxide on Mars. *Mars* **1992**, 934–968. Available online: <https://ui.adsabs.harvard.edu/abs/1992mars.book..934J/abstract> (accessed on 5 December 2021).
7. Buratti, B.J.; Cruikshank, D.P.; Brown, R.H.; Clark, R.N.; Bauer, J.M.; Jaumann, R.; McCord, T.B.; Simonelli, D.P.; Hibbitts, C.A.; Hansen, G.B.; et al. Cassini visual and infrared mapping spectrometer observations of Iapetus: Detection of CO<sub>2</sub>. *Astrophys. J. Lett.* **2005**, *622*, L149. [[CrossRef](#)]
8. Collins, G.; Johnson, T.V. Ganymede and Callisto. In *Encyclopedia of the Solar System*, 3th ed.; Elsevier: Amsterdam, The Netherlands, 2014; pp. 813–829.
9. Clark, R.N.; Cruikshank, D.P.; Jaumann, R.; Brown, R.H.; Stephan, K.; Dalle Ore, C.M.; Livo, K.; Pearson, N.; Curchin, J.; Hoefen, T.; et al. The surface composition of Iapetus: Mapping results from Cassini VIMS. *Icarus* **2012**, *218*, 831–860. [[CrossRef](#)]
10. Brown, R.H.; Baines, K.H.; Bellucci, G.; Buratti, B.J.; Capaccioni, F.; Cerroni, P.; Clark, R.; Coradini, A.; Cruikshank, D.; Drossart, P.; et al. Observations in the Saturn system during approach and orbital insertion, with Cassini's visual and infrared mapping spectrometer (VIMS). *Astron. Astrophys.* **2006**, *446*, 707–716. [[CrossRef](#)]
11. Grundy, W.M.; Young, L.A.; Stansberry, J.A.; Buie, M.W.; Olkin, C.B.; Young, E.F. Near-infrared spectral monitoring of Triton with IRTF/SpeX II: Spatial distribution and evolution of ices. *Icarus* **2010**, *205*, 594–604. [[CrossRef](#)]
12. Rubanenko, L.; Mazarico, E.; Neumann, G.A.; Paige, D.A. Ice in micro cold traps on Mercury: Implications for age and origin. *J. Geophys. Res. Planets* **2018**, *123*, 2178–2191. [[CrossRef](#)]
13. Williams, J.P.; Paige, D.A.; Greenhagen, B.T.; Sefton-Nash, E. The global surface temperatures of the Moon as measured by the Diviner Lunar Radiometer Experiment. *Icarus* **2017**, *283*, 300–325. [[CrossRef](#)]
14. Colaprete, A.; Schultz, P.; Heldmann, J.; Wooden, D.; Shirley, M.; Ennico, K.; Hermalyn, B.; Marshall, W.; Ricco, A.; Elphic, R.; et al. Detection of water in the LCROSS ejecta plume. *Science* **2010**, *330*, 463–468. [[CrossRef](#)]
15. Gladstone, G.R.; Hurley, D.M.; Retherford, K.D.; Feldman, P.D.; Pryor, W.R.; Chaufray, J.Y.; Versteeg, M.; Greathouse, T.; Steffl, A.; Throop, H.; et al. LRO-LAMP observations of the LCROSS impact plume. *Science* **2010**, *330*, 472–476. [[CrossRef](#)]
16. Haskin, L.; Warren, P. *Lunar Chemistry. Chapter 8 in "Lunar Sourcebook"*; Cambridge University Press: Cambridge, UK, 1991.
17. Zhang, J.A.; Paige, D.A. Cold-trapped organic compounds at the poles of the Moon and Mercury: Implications for origins. *Geophys. Res. Lett.* **2009**, *36*, 5. [[CrossRef](#)]
18. Schorghofer, N.; Byrne, S.; Landis, M.E.; Mazarico, E.; Prettyman, T.H.; Schmidt, B.E.; Villarreal, M.; Castillo-Rogez, J.; Raymond, C.; Russell, C.T. The putative Cerean exosphere. *Astrophys. J.* **2017**, *850*, 85. [[CrossRef](#)]
19. Slade, M.A.; Butler, B.J.; Muhleman, D.O. Mercury radar imaging: Evidence for polar ice. *Science* **1992**, *258*, 635–640. [[CrossRef](#)] [[PubMed](#)]
20. Phillips, R.J.; Davis, B.J.; Tanaka, K.L.; Byrne, S.; Mellon, M.T.; Putzig, N.E.; Haberle, R.; Kahre, M.; Campbell, B.; Carter, L.; et al. Massive CO<sub>2</sub> ice deposits sequestered in the south polar layered deposits of Mars. *Science* **2011**, *332*, 838–841. [[CrossRef](#)]
21. Howard, A.D. The role of eolian processes in forming surface features of the Martian polar layered deposits. *Icarus* **2000**, *144*, 267–288. [[CrossRef](#)]
22. Kieffer, H.H. Cold jets in the Martian polar caps. *J. Geophys. Res. Planets* **2007**, *112*. [[CrossRef](#)]
23. Piqueux, S.; Christensen, P.R. Deposition of CO<sub>2</sub> and erosion of the Martian south perennial cap between 1972 and 2004: Implications for current climate change. *J. Geophys. Res. Planets* **2008**, *113*. [[CrossRef](#)]
24. Johnson, R.E.; Carlson, R.W.; Cooper, J.F.; Paranicas, C.; Moore, M.H.; Wong, M.C. Radiation effects on the surfaces of the Galilean satellites. *Jupiter Planet Satellites Magnetosphere*. 2004, pp. 485–512. Available online: [https://lasp.colorado.edu/home/mop/files/2015/08/jupiter\\_ch20-1.pdf](https://lasp.colorado.edu/home/mop/files/2015/08/jupiter_ch20-1.pdf) (accessed on 5 December 2021).
25. Lebofsky, L.A. Stability of frosts in the solar system. *Icarus* **1975**, *25*, 205–217. [[CrossRef](#)]
26. Cartwright, R.J.; Emery, J.P.; Rivkin, A.S.; Trilling, D.E.; Pinilla-Alonso, N. Distribution of CO<sub>2</sub> ice on the large moons of Uranus and evidence for compositional stratification of their near-surfaces. *Icarus* **2015**, *257*, 428–456. [[CrossRef](#)]
27. Kubo, T.; Nakata, H.; Kato, T. Effects of insoluble particles on grain growth in polycrystalline ice: Implications for rheology of ice shells of icy satellites. *J. Mineral. Petrol. Sci.* **2009**, *104*, 301–306. [[CrossRef](#)]
28. Umurhan, O.M.; Ahrens, C.J.; Chevrier, V.F. Rheological and Thermophysical Properties and Some Processes Involving Common Volatile Materials Found on Pluto's Surface. *Pluto Syst. After New Horiz.* **2021**, 195–255.
29. Hapke, B. *Theory of Reflectance and Emittance Spectroscopy*; Cambridge University Press: Cambridge, UK, 2012.
30. Moore, J.M.; Howard, A.D.; Umurhan, O.M.; White, O.L.; Schenk, P.M.; Beyer, R.A.; McKinnon, W.B.; Spencer, J.R.; Grundy, W.M.; Lauer, T.R.; et al. Sublimation as a landform-shaping process on Pluto. *Icarus* **2017**, *287*, 320–333. [[CrossRef](#)]
31. Byrne, S.; Ingersoll, A.P. A sublimation model for Martian south polar ice features. *Science* **2003**, *299*, 1051–1053. [[CrossRef](#)]
32. Bertrand, T.; Forget, F. Observed glacier and volatile distribution on Pluto from atmosphere–topography processes. *Nature* **2016**, *540*, 86–89. [[CrossRef](#)]
33. Grundy, W.M.; Binzel, R.P.; Buratti, B.J.; Cook, J.C.; Cruikshank, D.P.; Dalle Ore, C.M.; Earle, A.M.; Ennico, K.; Howett, C.A.; Lunsford, A.W.; et al. Surface compositions across Pluto and Charon. *Science* **2016**, *351*, aad9189. [[CrossRef](#)]

34. Squyres, S.W. Ganymede and Callisto: One of Jupiter's icy moons shows evidence of a period of intense geologic activity, whereas the other appears to have remained dormant. *Am. Sci.* **1983**, *71*, 56–64.
35. De Bergh, C.; Schmitt, B.; Moroz, L.V.; Quirico, E.; Cruikshank, D.P. Laboratory data on ices, refractory carbonaceous materials, and minerals relevant to transneptunian objects and Centaurs. In *The Solar System Beyond Neptune*; University of Arizona: Tucson, AZ, USA, 2008; pp. 483–506.
36. Barrett, C.S.; Meyer, L. Phase Diagram of Argon—Carbon Monoxide. *J. Chem. Phys.* **1965**, *43*, 3502–3506. [[CrossRef](#)]
37. Quirico, E.; Schmitt, B. Near-Infrared Spectroscopy of Simple Hydrocarbons and Carbon Oxides Diluted in Solid N<sub>2</sub> and as Pure Ices: Implications for Triton and Pluto. *Icarus* **1997**, *127*, 354–378. [[CrossRef](#)]
38. Fray, N.; Schmitt, B. Sublimation of ices of astrophysical interest: A bibliographic review. *Planet. Space Sci.* **2009**, *57*, 2053–2080. [[CrossRef](#)]
39. Sori, M.M.; Bapst, J.; Bramson, A.M.; Byrne, S.; Landis, M.E. A Wunda-full world? Carbon dioxide ice deposits on Umbriel and other Uranian moons. *Icarus* **2017**, *290*, 1–13. [[CrossRef](#)]
40. Gerakines, P.A.; Hudson, R.L. First infrared band strengths for amorphous CO<sub>2</sub>, an overlooked component of interstellar ices. *Astrophys. J. Lett.* **2015**, *808*, L40. [[CrossRef](#)]
41. Satorre, M.Á.; Domingo, M.; Millán, C.; Luna, R.; Vilaplana, R.; Santonja, C. Density of CH<sub>4</sub>, N<sub>2</sub> and CO<sub>2</sub> ices at different temperatures of deposition. *Planet. Space Sci.* **2008**, *56*, 1748–1752. [[CrossRef](#)]
42. Jiang, G.J.; Person, W.B.; Brown, K.G. Absolute infrared intensities and band shapes in pure solid CO and CO in some solid matrices. *J. Chem. Phys.* **1975**, *62*, 1201–1211. [[CrossRef](#)]
43. Jamieson, C.S.; Mebel, A.M.; Kaiser, R.I. Understanding the kinetics and dynamics of radiation-induced reaction pathways in carbon monoxide ice at 10 K. *Astrophys. J. Suppl. Ser.* **2006**, *163*, 184. [[CrossRef](#)]
44. Satorre, M.Á.; Luna, R.; Millán, C.; Domingo, M.; Santonja, C. Density of ices of astrophysical interest. In *Laboratory Astrophysics*; Springer: Cham, Switzerland, 2018; pp. 51–69.
45. Moore, J.M.; McKinnon, W.B.; Spencer, J.R.; Howard, A.D.; Schenk, P.M.; Beyer, R.A.; Nimmo, F.; Singer, K.; Umurhan, O.; White, O.; et al. The geology of Pluto and Charon through the eyes of New Horizons. *Science* **2016**, *351*, 1284–1293. [[CrossRef](#)] [[PubMed](#)]
46. Musiolik, G.; Teiser, J.; Jankowski, T.; Wurm, G. Collisions of CO<sub>2</sub> ice grains in planet formation. *Astrophys. J.* **2016**, *818*, 16. [[CrossRef](#)]
47. Luna, R.; Satorre, M.Á.; Santonja, C.; Domingo, M. New experimental sublimation energy measurements for some relevant astrophysical ices. *Astron. Astrophys.* **2014**, *566*, A27. [[CrossRef](#)]
48. Schmitt, B.; Espinasse, S.; Grim, R.J.A.; Greenberg, J.M.; Klinger, J. Laboratory studies of cometary ice analogues. In *Physics and Mechanics of Cometary Materials*, European Space Agency, Münster, FRG; European Space Agency: Paris, France, 1989; Volume 302, Available online: [https://inis.iaea.org/collection/NCLCollectionStore/\\_Public/21/088/21088789.pdf](https://inis.iaea.org/collection/NCLCollectionStore/_Public/21/088/21088789.pdf) (accessed on 5 December 2021).
49. Delitsky, M.L.; Lane, A.L. Ice chemistry on the Galilean satellites. *J. Geophys. Res. Planets* **1998**, *103*, 31391–31403. [[CrossRef](#)]
50. Teolis, B.D.; Waite, J.H. Dione and Rhea seasonal exospheres revealed by Cassini CAPS and INMS. *Icarus* **2016**, *272*, 277–289. [[CrossRef](#)]
51. Cruikshank, D.P.; Meyer, A.W.; Brown, R.H.; Clark, R.N.; Jaumann, R.; Stephan, K.; Hibbitts, C.; Sandford, S.; Mastrapa, R.; Filacchione, G.; et al. Carbon dioxide on the satellites of Saturn: Results from the Cassini VIMS investigation and revisions to the VIMS wavelength scale. *Icarus* **2010**, *206*, 561–572. [[CrossRef](#)]
52. Palumbo, M.E.; Strazzulla, G. The 2140/cm band of frozen CO-Laboratory experiments and astrophysical applications. *Astron. Astrophys.* **1993**, *269*, 568–580.
53. Sandford, S.A.; Allamandola, L.J.; Tielens, A.G.G.M.; Valero, G.J. Laboratory studies of the infrared spectral properties of CO in astrophysical ices. *Astrophys. J.* **1988**, *329*, 498–510. [[CrossRef](#)]
54. Journaux, B.; Kalousova, K.; Sotin, C.; Tobie, G.; Vance, S.; Saur, J.; Bollengier, O.; Noack, L.; Ruckriemen-Bez, T.; Van Hoolst, T.; et al. Large ocean worlds with high-pressure ices. *Space Sci. Rev.* **2020**, *216*, 1–36. [[CrossRef](#)]
55. Ehrenfreund, P.; Kerkhof, O.; Schutte, W.A.; Boogert, A.C.A.; Gerakines, P.A.; Dartois, E.; d'Hendecourt, L.; Tielens, A.; van Dishoeck, E.; Whittet, D.C.B. Laboratory studies of thermally processed H<sub>2</sub>O-CH<sub>3</sub>OH-CO<sub>2</sub> ice mixtures and their astrophysical implications. *Astron. Ap.* **1999**, *350*, 240–253.
56. Gibb, E.L.; Whittet, D.C.B.; Boogert, A.C.A.; Tielens, A.G.G.M. Interstellar ice: The infrared space observatory legacy. *Astrophys. J. Suppl. Ser.* **2004**, *151*, 35. [[CrossRef](#)]
57. Raut, U.; Fulvio, D.; Loeffler, M.J.; Baragiola, R.A. Radiation synthesis of carbon dioxide in ice-coated carbon: Implications for interstellar grains and icy moons. *Astrophys. J.* **2012**, *752*, 159. [[CrossRef](#)]
58. Ferrari, B.C.; Slavicinska, K.; Bennett, C.J. Role of Suprathermal Chemistry on the Evolution of Carbon Oxides and Organics within Interstellar and Cometary Ices. *Acc. Chem. Res.* **2021**, *54*, 1067–1079. [[CrossRef](#)]
59. Raut, U.; Baragiola, R.A. Solid-state CO oxidation by atomic O: A route to solid CO<sub>2</sub> synthesis in dense molecular clouds. *Astrophys. J. Lett.* **2011**, *737*, L14. [[CrossRef](#)]
60. Mennella, V.; Baratta, G.A.; Palumbo, M.E.; Bergin, E.A. Synthesis of CO and CO<sub>2</sub> molecules by UV irradiation of water ice-covered hydrogenated carbon grains. *Astrophys. J.* **2006**, *643*, 923. [[CrossRef](#)]

61. Bennett, C.J.; Jamieson, C.S.; Kaiser, R.I. Mechanistical studies on the formation and destruction of carbon monoxide (CO), carbon dioxide (CO<sub>2</sub>), and carbon trioxide (CO<sub>3</sub>) in interstellar ice analog samples. *Phys. Chem. Chem. Phys.* **2010**, *12*, 4032–4050. [[CrossRef](#)]
62. Kaiser, R.I. Experimental investigation on the formation of carbon-bearing molecules in the interstellar medium via neutral–neutral reactions. *Chem. Rev.* **2002**, *102*, 1309–1358. [[CrossRef](#)]
63. Bennett, C.J.; Brotton, S.J.; Jones, B.M.; Misra, A.K.; Sharma, S.K.; Kaiser, R.I. High-sensitivity raman spectrometer to study pristine and irradiated interstellar ice analogs. *Anal. Chem.* **2013**, *85*, 5659–5665. [[CrossRef](#)] [[PubMed](#)]
64. Loeffler, M.J.; Baratta, G.A.; Palumbo, M.E.; Strazzulla, G.; Baragiola, R.A. CO synthesis in solid CO by Lyman- $\alpha$  photons and 200 keV protons. *Astron. Astrophys.* **2005**, *435*, 587–594. [[CrossRef](#)]
65. Gerakines, P.A.; Moore, M.H.; Hudson, R.L. Energetic processing of laboratory ice analogs: UV photolysis versus ion bombardment. *J. Geophys. Res. Planets* **2001**, *106*, 33381–33385. [[CrossRef](#)]
66. Satorre, M.A.; Palumbo, M.E.; Strazzulla, G. CO/CO<sub>2</sub> Molecular Number Ratio Produced by ion Irradiation of Ices. *Astrophys. Space Sci.* **2000**, *274*, 643–653. [[CrossRef](#)]
67. Mennella, V.; Palumbo, M.E.; Baratta, G.A. Formation of CO and CO<sub>2</sub> molecules by ion irradiation of water ice-covered hydrogenated carbon grains. *Astrophys. J.* **2004**, *615*, 1073. [[CrossRef](#)]
68. Gomis, O.; Strazzulla, G. CO<sub>2</sub> production by ion irradiation of H<sub>2</sub>O ice on top of carbonaceous materials and its relevance to the Galilean satellites. *Icarus* **2005**, *177*, 570–576. [[CrossRef](#)]
69. Kim, Y.S.; Kaiser, R.I. Electron irradiation of Kuiper belt surface ices: Ternary N<sub>2</sub>-CH<sub>4</sub>-CO mixtures as a case study. *Astrophys. J.* **2012**, *758*, 37. [[CrossRef](#)]
70. Shi, J.; Grieves, G.A.; Orlando, T.M. Vacuum ultraviolet photon-stimulated oxidation of buried ice: Graphite grain interfaces. *Astrophys. J.* **2015**, *804*, 24. [[CrossRef](#)]
71. Sabri, T.; Baratta, G.A.; Jäger, C.; Palumbo, M.E.; Henning, T.; Strazzulla, G.; Wendler, E. A laboratory study of ion-induced erosion of ice-covered carbon grains. *Astron. Astrophys.* **2015**, *575*, A76. [[CrossRef](#)]
72. Baragiola, R.A. Energetic electronic processes on extraterrestrial surfaces. *Nucl. Instrum. Methods Phys. Res. Sect. B Beam Interact. Mater. At.* **2005**, *232*, 98–107. [[CrossRef](#)]
73. Moore, M.H.; Hudson, R.L. IR detection of H<sub>2</sub>O<sub>2</sub> at 80 K in ion-irradiated laboratory ices relevant to Europa. *Icarus* **2000**, *145*, 282–288. [[CrossRef](#)]
74. Kaiser, P.; Unde, R.B.; Kern, C.; Jess, A. Production of liquid hydrocarbons with CO<sub>2</sub> as carbon source based on reverse water-gas shift and Fischer-Tropsch synthesis. *Chem. Ing. Tech.* **2013**, *85*, 489–499. [[CrossRef](#)]
75. Strazzulla, G.; Baratta, G.A.; Palumbo, M.E. Vibrational spectroscopy of ion-irradiated ices. *Spectrochim. Acta Part A Mol. Biomol. Spectrosc.* **2001**, *57*, 825–842. [[CrossRef](#)]
76. Brucato, J.R.; Castorina, A.C.; Palumbo, M.E.; Satorre, M.A.; Strazzulla, G. Ion irradiation and extended CO emission in cometary comae. *Planet. Space Sci.* **1997**, *45*, 835–840. [[CrossRef](#)]
77. Brucato, J.R.; Palumbo, M.E.; Strazzulla, G. Carbonic acid by ion implantation in water/carbon dioxide ice mixtures. *Icarus* **1997**, *125*, 135–144. [[CrossRef](#)]
78. Hand, K.P.; Carlson, R.W. H<sub>2</sub>O<sub>2</sub> production by high-energy electrons on icy satellites as a function of surface temperature and electron flux. *Icarus* **2011**, *215*, 226–233. [[CrossRef](#)]
79. Johnson, R.E.; Quickenden, T.I.; Cooper, P.D.; McKinley, A.J.; Freeman, C.G. The production of oxidants in Europa’s surface. *Astrobiology* **2003**, *3*, 823–850. [[CrossRef](#)]
80. Moore, M.H.; Khanna, R.; Donn, B. Studies of proton irradiated H<sub>2</sub>O+ CO<sub>2</sub> and H<sub>2</sub>O+ CO ices and analysis of synthesized molecules. *J. Geophys. Res. Planets* **1991**, *96*, 17541–17545. [[CrossRef](#)]
81. Mura, A.; Adriani, A.; Sordini, R.; Sindoni, G.; Plainaki, C.; Tosi, F.; Filacchione, G.; Bolton, S.; Zambon, F.; Hansen, C.; et al. Infrared Observations of Ganymede From the Jovian InfraRed Auroral Mapper on Juno. *J. Geophys. Res. Planets* **2020**, *125*, e2020JE006508. [[CrossRef](#)]
82. Carlson, R.W.; Weissman, P.R.; Smythe, W.D.; Mahoney, J.C. Near-infrared mapping spectrometer experiment on Galileo. *Space Sci. Rev.* **1992**, *60*, 457–502. [[CrossRef](#)]
83. Brown, R.H.; Baines, K.H.; Bellucci, G.; Bibring, J.P.; Buratti, B.J.; Capaccioni, F.; Cerroni, P.; Clark, R.; Coradini, A.; Cruikshank, D.; et al. The Cassini visual and infrared mapping spectrometer (VIMS) investigation. *Space Sci. Rev.* **2004**, *115*, 111–168. [[CrossRef](#)]
84. Schmitt, B.; Philippe, S.; Grundy, W.M.; Reuter, D.C.; Côte, R.; Quirico, E.; Protopapa, S.; Young, L.; Binzel, R.; Cook, J.; et al. Physical state and distribution of materials at the surface of Pluto from New Horizons LEISA imaging spectrometer. *Icarus* **2017**, *287*, 229–260. [[CrossRef](#)]
85. McCord, T.A.; Hansen, G.B.; Clark, R.N.; Martin, P.D.; Hibbitts, C.A.; Fanale, F.P.; Granahan, J.; Segura, M.; Matson, D.; Johnson, T.; et al. Non-water-ice constituents in the surface material of the icy Galilean satellites from the Galileo near-infrared mapping spectrometer investigation. *J. Geophys. Res. Planets* **1998**, *103*, 8603–8626. [[CrossRef](#)]
86. Isokoski, K.; Poteet, C.A.; Linnartz, H. Highly resolved infrared spectra of pure CO<sub>2</sub> ice (15–75 K). *Astron. Astrophys.* **2013**, *555*, A85. [[CrossRef](#)]
87. Hibbitts, C.A.; Szanyi, J. Physisorption of CO<sub>2</sub> on non-ice materials relevant to icy satellites. *Icarus* **2007**, *191*, 371–380. [[CrossRef](#)]
88. Baratta, G.A.; Palumbo, M.E. Infrared optical constants of CO and CO<sub>2</sub> thin icy films. *JOSA A* **1998**, *15*, 3076–3085. [[CrossRef](#)]

89. Bernstein, M.P.; Cruikshank, D.P.; Sandford, S.A. Near-infrared laboratory spectra of solid H<sub>2</sub>O/CO<sub>2</sub> and CH<sub>3</sub>OH/CO<sub>2</sub> ice mixtures. *Icarus* **2005**, *179*, 527–534. [[CrossRef](#)]
90. Schmitt, B. The Solid Spectroscopy Data Model (SSDM) and the GhoSST Database. In *EPSC-DPS Joint Meeting 2011*, 2011; Volume 2011, p. 1475. Available online: <https://ghosst.osug.fr/search/band> (accessed on 5 December 2021).
91. McCord, T.A.; Carlson, R.W.; Smythe, W.D.; Hansen, G.B.; Clark, R.N.; Hibbitts, C.A.; Fanale, F.; Granahan, J.; Segura, M.; Matson, D.; et al. Organics and other molecules in the surfaces of Callisto and Ganymede. *Science* **1997**, *278*, 271–275. [[CrossRef](#)] [[PubMed](#)]
92. Hibbitts, C.A.; Pappalardo, R.T.; Hansen, G.B.; McCord, T.B. Carbon dioxide on Ganymede. *J. Geophys. Res. Planets* **2003**, *108*, 5036. [[CrossRef](#)]
93. Clark, R.N.; Brown, R.H.; Cruikshank, D.P.; Swayze, G.A. Isotopic ratios of Saturn's rings and satellites: Implications for the origin of water and Phoebe. *Icarus* **2019**, *321*, 791–802. [[CrossRef](#)]
94. Douté, S.; Schmitt, B.; Quirico, E.; Owen, T.C.; Cruikshank, D.P.; De Bergh, C.; Geballe, T.; Roush, T.L. Evidence for methane segregation at the surface of Pluto. *Icarus* **1999**, *142*, 421–444. [[CrossRef](#)]
95. Gerakines, P.A.; Bray, J.J.; Davis, A.; Richey, C.R. The strengths of near-infrared absorption features relevant to interstellar and planetary ices. *Astrophys. J.* **2005**, *620*, 1140. [[CrossRef](#)]
96. Nelson, R.M.; Lane, A.L.; Matson, D.L.; Veeder, G.J.; Buratti, B.J.; Tedesco, E.F. Spectral geometric albedos of the Galilean satellites from 0.24 to 0.34 micrometers: Observations with the International Ultraviolet Explorer. *Icarus* **1987**, *72*, 358–380. [[CrossRef](#)]
97. Spencer, J.R.; Calvin, W.M.; Person, M.J. Charge-coupled device spectra of the Galilean satellites: Molecular oxygen on Ganymede. *J. Geophys. Res. Planets* **1995**, *100*, 19049–19056. [[CrossRef](#)]
98. Spencer, J.R. Thermal segregation of water ice on the Galilean satellites. *Icarus* **1987**, *69*, 297–313. [[CrossRef](#)]
99. Orton, G.S.; Spencer, J.R.; Travis, L.D.; Martin, T.Z.; Tamppari, L.K. Galileo photopolarimeter-radiometer observations of Jupiter and the Galilean satellites. *Science* **1996**, *274*, 389–391. [[CrossRef](#)]
100. Hudson, R.L.; Moore, M.H. Far-IR spectral changes accompanying proton irradiation of solids of astrochemical interest. *Radiat. Phys. Chem.* **1995**, *45*, 779–789. [[CrossRef](#)]
101. Carlson, R.; Smythe, W.; Baines, K.; Barbinis, E.; Becker, K.; Burns, R.; Calcutt, S.; Calvin, W.; Clark, R.; Danielson, G.; et al. Near-infrared spectroscopy and spectral mapping of Jupiter and the Galilean satellites: Results from Galileo's initial orbit. *Science* **1996**, *274*, 385–388. [[CrossRef](#)]
102. Pappalardo, R.T.; Collins, G.C.; Head, J.W.; Helfenstein, P.; McCord, T.B.; Moore, J.M.; Prockter, L.; Schenk, P.; Spencer, J.R. Geology of ganymede. *Jupit. Planet Satell. Magnetos.* **2004**, *2*, 363.
103. Hibbitts, C.A.; Klemaszewski, J.E.; McCord, T.B.; Hansen, G.B.; Greeley, R. CO<sub>2</sub>-rich impact craters on Callisto. *J. Geophys. Res. Planets* **2002**, *107*, 14-1–14-12. [[CrossRef](#)]
104. Hibbitts, C.A.; McCord, T.B.; Hansen, G.B. Distributions of CO<sub>2</sub> and SO<sub>2</sub> on the surface of Callisto. *J. Geophys. Res. Planets* **2000**, *105*, 22541–22557. [[CrossRef](#)]
105. Jewitt, D. From comets to asteroids: When hairy stars go bald. In *Worlds in Interaction: Small Bodies and Planets of the Solar System*; Springer: Dordrecht, The Netherlands, 1996; pp. 185–201.
106. Carlson, R.W.; Johnson, R.E.; Anderson, M.S. Sulfuric acid on Europa and the radiolytic sulfur cycle. *Science* **1999**, *286*, 97–99. [[CrossRef](#)] [[PubMed](#)]
107. Miller, S.L. Clathrate hydrates in the solar system. In *Ices in the Solar System*; Springer: Dordrecht, The Netherlands, 1985; pp. 59–79.
108. Kargel, J.S.; Lunine, J.I. Clathrate hydrates on Earth and in the solar system. In *Solar System Ices*; Springer: Dordrecht, The Netherlands, 1998; pp. 97–117.
109. Kargel, J.S.; Kaye, J.Z.; Head III, J.W.; Marion, G.M.; Sassen, R.; Crowley, J.K.; Ballesteros, O.; Grant, S.; Hogenboom, D.L. Europa's crust and ocean: Origin, composition, and the prospects for life. *Icarus* **2000**, *148*, 226–265. [[CrossRef](#)]
110. Zolotov, M.Y.; Shock, E.L. Composition and stability of salts on the surface of Europa and their oceanic origin. *J. Geophys. Res. Planets* **2001**, *106*, 32815–32827. [[CrossRef](#)]
111. Chyba, C.F. Energy for microbial life on Europa. *Nature* **2000**, *403*, 381–382. [[CrossRef](#)]
112. Hand, K.P.; Chyba, C.F.; Carlson, R.W.; Cooper, J.F. Clathrate hydrates of oxidants in the ice shell of Europa. *Astrobiology* **2006**, *6*, 463–482. [[CrossRef](#)]
113. Nordheim, T.A.; Hand, K.P.; Paranicas, C. Preservation of potential biosignatures in the shallow subsurface of Europa. *Nat. Astron.* **2018**, *2*, 673–679. [[CrossRef](#)]
114. Hall, D.T.; Strobel, D.F.; Feldman, P.D.; McGrath, M.A.; Weaver, H.A. Detection of an oxygen atmosphere on Jupiter's moon Europa. *Nature* **1995**, *373*, 677–679. [[CrossRef](#)]
115. Hansen, G.B.; McCord, T.B. Widespread CO<sub>2</sub> and other non-ice compounds on the anti-Jovian and trailing sides of Europa from Galileo/NIMS observations. *Geophys. Res. Lett.* **2008**, *35*, 1. [[CrossRef](#)]
116. McCord, T.B.; Hansen, G.B.; Fanale, F.P.; Carlson, R.W.; Matson, D.L.; Johnson, T.V.; Smythe, W.; Crowley, J.; Martin, P.; Ocampo, A.; et al. Salts on Europa's surface detected by Galileo's near infrared mapping spectrometer. *Science* **1998**, *280*, 1242–1245. [[CrossRef](#)]
117. McCord, T.B.; Hansen, G.B.; Matson, D.L.; Johnson, T.V.; Crowley, J.K.; Fanale, F.P.; Carlson, R.; Smythe, W.; Martin, P.; Hibbitts, C.; et al. Hydrated salt minerals on Europa's surface from the Galileo near-infrared mapping spectrometer (NIMS) investigation. *J. Geophys. Res. Planets* **1999**, *104*, 11827–11851. [[CrossRef](#)]

118. Oancea, A.; Grasset, O.; Le Menn, E.; Bollengier, O.; Bezacier, L.; Le Mouélic, S.; Tobie, G. Laboratory infrared reflection spectrum of carbon dioxide clathrate hydrates for astrophysical remote sensing applications. *Icarus* **2012**, *221*, 900–910. [[CrossRef](#)]
119. Bouquet, A.; Mousis, O.; Glein, C.R.; Danger, G.; Waite, J.H. The role of clathrate formation in Europa's ocean composition. *Astrophys. J.* **2019**, *885*, 14. [[CrossRef](#)]
120. Shock, E.L. Chemical environments of submarine hydrothermal systems. *Mar. Hydrothermal Syst. Orig. Life* **1992**, 67–107. [[CrossRef](#)]
121. Nash, D.B.; Nelson, R.M. Spectral evidence for sublimates and adsorbates on Io. *Nature* **1979**, *280*, 763–766. [[CrossRef](#)]
122. Trafton, L.M.; Lester, D.F.; Ramseyer, T.F.; Salama, F.; Sanford, S.A.; Allamandola, L.J. A new class of absorption feature in Io's near-infrared spectrum. *Icarus* **1991**, *89*, 264–276. [[CrossRef](#)]
123. Sandford, S.A.; Salama, F.; Allamandola, L.J.; Trafton, L.M.; Lester, D.F.; Ramseyer, T.F. Laboratory studies of the newly discovered infrared band at 4705.2 cm<sup>-1</sup> (2.1253 μm) in the spectrum of Io: The tentative identification of CO<sub>2</sub>. *Icarus* **1991**, *91*, 125–144. [[CrossRef](#)]
124. Sandford, S.A.; Allamandola, L.J. The condensation and vaporization behavior of ices containing SO<sub>2</sub>, H<sub>2</sub>S, and CO<sub>2</sub>: Implications for Io. *Icarus* **1993**, *106*, 478–488. [[CrossRef](#)] [[PubMed](#)]
125. Salama, F.; Allamandola, L.J.; Witteborn, F.C.; Cruikshank, D.P.; Sandford, S.A.; Bregman, J.D. The 2.5–5.0 μm spectra of Io: Evidence for H<sub>2</sub>S and H<sub>2</sub>O frozen in SO<sub>2</sub>. *Icarus* **1990**, *83*, 66–82. [[CrossRef](#)]
126. Clark, R.N.; Curchin, J.M.; Jaumann, R.; Cruikshank, D.P.; Brown, R.H.; Hoefen, T.M.; Steohan, K.; Moore, J.; Buratti, B.; Baines, K.; et al. Compositional mapping of Saturn's satellite Dione with Cassini VIMS and implications of dark material in the Saturn system. *Icarus* **2008**, *193*, 372–386. [[CrossRef](#)]
127. Waite, J.H.; Combi, M.R.; Ip, W.H.; Cravens, T.E.; McNutt, R.L.; Kasprzak, W.; Yelle, R.; Luhmann, J.; Niemann, H.; Gell, D.; et al. Cassini ion and neutral mass spectrometer: Enceladus plume composition and structure. *Science* **2006**, *311*, 1419–1422. [[CrossRef](#)]
128. Palmer, E.E.; Brown, R.H. Production and detection of carbon dioxide on Iapetus. *Icarus* **2011**, *212*, 807–818. [[CrossRef](#)]
129. Cassidy, T.; Coll, P.; Raulin, F.; Carlson, R.W.; Johnson, R.E.; Loeffler, M.J.; Hand, K.; Baragiola, R.A. Radiolysis and photolysis of icy satellite surfaces: Experiments and theory. *Space Sci. Rev.* **2010**, *153*, 299–315. [[CrossRef](#)]
130. Pinilla-Alonso, N.; Roush, T.L.; Marzo, G.A.; Cruikshank, D.P.; Dalle Ore, C.M. Iapetus surface variability revealed from statistical clustering of a VIMS mosaic: The distribution of CO<sub>2</sub>. *Icarus* **2011**, *215*, 75–82. [[CrossRef](#)]
131. Teolis, B.D.; Perry, M.E.; Hansen, C.J.; Waite, J.H.; Porco, C.C.; Spencer, J.R.; Howett, C.J. Enceladus plume structure and time variability: Comparison of Cassini observations. *Astrobiology* **2017**, *17*, 926–940. [[CrossRef](#)]
132. Combe, J.P.; McCord, T.B.; Matson, D.L.; Johnson, T.V.; Davies, A.G.; Scipioni, F.; Tosi, F. Nature, distribution and origin of CO<sub>2</sub> on Enceladus. *Icarus* **2014**, *317*, 491–508. [[CrossRef](#)]
133. Prasad, P.S.R.; Prasad, K.S.; Thakur, N.K. FTIR signatures of type-II clathrates of carbon dioxide in natural quartz veins. *Curr. Sci.* **2006**, *90*, 1544–1547.
134. Moore, J.M.; Mellon, M.T.; Zent, A.P. Mass wasting and ground collapse in terrains of volatile-rich deposits as a solar system-wide geological process: The pre-Galileo view. *Icarus* **1996**, *122*, 63–78. [[CrossRef](#)]
135. Blake, D.; Allamandola, L.; Sandford, S.; Hudgins, D.; Freund, F. Clathrate hydrate formation in amorphous cometary ice analogs in vacuo. *Science* **1991**, *254*, 548–551. [[CrossRef](#)] [[PubMed](#)]
136. Ali-Dib, M.; Mousis, O.; Petit, J.M.; Lunine, J.I. The measured compositions of Uranus and Neptune from their formation on the CO ice line. *Astrophys. J.* **2014**, *793*, 9. [[CrossRef](#)]
137. Cartwright, R.; Emery, J.P. Compositional Trends on the Large Moons of Uranus: Evidence for System-Wide Modification. In *AGU Fall Meeting Abstracts*; AGU: New Orleans, LA, USA, 2017; Volume 2017, p. P31D-2861.
138. Grundy, W.M.; Young, L.A.; Spencer, J.R.; Johnson, R.E.; Young, E.F.; Buie, M.W. Distributions of H<sub>2</sub>O and CO<sub>2</sub> ices on Ariel, Umbriel, Titania, and Oberon from IRTF/SpeX observations. *Icarus* **2006**, *184*, 543–555. [[CrossRef](#)]
139. Plescia, J.B. Geological terrains and crater frequencies on Ariel. *Nature* **1987**, *327*, 201–204. [[CrossRef](#)]
140. Zahnle, K.; Schenk, P.; Levison, H.; Dones, L. Cratering rates in the outer Solar System. *Icarus* **2003**, *163*, 263–289. [[CrossRef](#)]
141. Cruikshank, D.P.; Brown, R.H.; Clark, R.N. Nitrogen on Triton. *Icarus* **1984**, *58*, 293–305. [[CrossRef](#)]
142. Cruikshank, D.P.; Roush, T.L.; Owen, T.C.; Geballe, T.R.; De Bergh, C.; Schmitt, B.; Brown, R.; Bartholomew, M.J. Ices on the surface of Triton. *Science* **1993**, *261*, 742–745. [[CrossRef](#)]
143. Quirico, E.; Douté, S.; Schmitt, B.; de Bergh, C.; Cruikshank, D.P.; Owen, T.C.; Geballe, T.; Roush, T.L. Composition, physical state, and distribution of ices at the surface of Triton. *Icarus* **1999**, *139*, 159–178. [[CrossRef](#)]
144. Tegler, S.C.; Stufflebeam, T.D.; Grundy, W.M.; Hanley, J.; Dustrud, S.; Lindberg, G.E.; Engle, A.; Dillingham, T.; Matthew, D.; Trilling, D.; et al. A New Two-molecule Combination Band as a Diagnostic of Carbon Monoxide Diluted in Nitrogen Ice on Triton. *Astron. J.* **2019**, *158*, 17. [[CrossRef](#)]
145. Lellouch, E.; Stansberry, J.; Emery, J.; Grundy, W.; Cruikshank, D.P. Thermal properties of Pluto's and Charon's surfaces from Spitzer observations. *Icarus* **2011**, *214*, 701–716. [[CrossRef](#)]
146. Quirico, E.; Schmitt, B. A Spectroscopic Study of CO Diluted in N<sub>2</sub>Ice: Applications for Triton and Pluto. *Icarus* **1997**, *128*, 181–188. [[CrossRef](#)]
147. Stern, S.A.; Bagenal, F.; Ennico, K.; Gladstone, G.R.; Grundy, W.M.; McKinnon, W.B.; Moore, J.; Olkin, C.; Spencer, J.; Weaver, H.; et al. The Pluto system: Initial results from its exploration by New Horizons. *Science* **2015**, *350*, 6258. [[CrossRef](#)]

148. White, O.L.; Moore, J.M.; McKinnon, W.B.; Spencer, J.R.; Howard, A.D.; Schenk, P.M.; Beyer, R.; Nimmo, F.; Singer, K.; Umurhan, O.; et al. Geological mapping of sputnik planitia on pluto. *Icarus* **2017**, *287*, 261–286. [[CrossRef](#)]
149. Womack, M.; Sarid, G.; Wierzbos, K. CO and other volatiles in distantly active comets. *Publ. Astron. Soc. Pac.* **2017**, *129*, 031001. [[CrossRef](#)]
150. Läuter, M.; Kramer, T.; Rubin, M.; Altwegg, K. Surface localization of gas sources on comet 67P/Churyumov–Gerasimenko based on DFMS/COPS data. *Mon. Not. R. Astron. Soc.* **2019**, *483*, 852–861. [[CrossRef](#)]
151. Ip, W.H. On photochemical heating of cometary comae—The cases of H<sub>2</sub>O and CO-rich comets. *Astrophys. J.* **1983**, *264*, 726–732. [[CrossRef](#)]
152. Huebner, W.F.; Carpenter, C.W. *Solar Photo Rate Coefficients*; Los Alamos Scientific Lab.: Los Alamos County, NM, USA, 1979; No. LA-8085-MS.
153. Wesołowski, M.; Gronkowski, P.; Tralle, I. Outbursts of comets at large heliocentric distances: Concise review and numerical simulations of brightness jumps. *Planet. Space Sci.* **2020**, *184*, 104867. [[CrossRef](#)]
154. Cochran, A.; Barker, E.S.; Cochran, W. Spectrophotometric observations of P/Schwassmann-Wachmann 1 during outburst. *Astron. J.* **1980**, *85*, 474–477. [[CrossRef](#)]
155. Bockelee-Morvan, D.; Debout, V.; Erard, S.; Leyrat, C.; Capaccioni, F.; Filacchione, G.; Fougere, N.; Drossart, P.; Arnold, G.; Combi, M.; et al. First observations of H<sub>2</sub>O and CO<sub>2</sub> vapor in comet 67P/Churyumov-Gerasimenko made by VIRTIS onboard Rosetta. *Astron. Astrophys.* **2015**, *583*, A6. [[CrossRef](#)]
156. Filacchione, G.; Capaccioni, F.; Ciarniello, M.; Raponi, A.; Tosi, F.; De Sanctis, M.C.; Erard, S.; Bocklee Morvan, D.; Leyrat, C.; Arnold, G.; et al. The global surface composition of 67P/CG nucleus by Rosetta/VIRTIS.(I) Prelanding mission phase. *Icarus* **2016**, *274*, 334–349. [[CrossRef](#)]
157. Hoang, M.; Garnier, P.; Gourlaouen, H.; Lasue, J.; Rème, H.; Altwegg, K.; Balsiger, H.; Beth, A.; Calmonte, U.; Fiethe, B.; et al. Two years with comet 67P/Churyumov-Gerasimenko: H<sub>2</sub>O, CO<sub>2</sub>, and CO as seen by the ROSINA/RTOF instrument of Rosetta. *Astron. Astrophys.* **2019**, *630*, A33. [[CrossRef](#)]
158. Fink, U.; Doose, L.; Rinaldi, G.; Bieler, A.; Capaccioni, F.; Bockelée-Morvan, D.; Filacchione, G.; Erard, S.; Leyrat, C.; Blecka, M.; et al. Investigation into the disparate origin of CO<sub>2</sub> and H<sub>2</sub>O outgassing for Comet 67/P. *Icarus* **2016**, *277*, 78–97. [[CrossRef](#)]
159. Läuter, M.; Kramer, T.; Rubin, M.; Altwegg, K. The gas production of 14 species from comet 67P/Churyumov–Gerasimenko based on DFMS/COPS data from 2014 to 2016. *Mon. Not. R. Astron. Soc.* **2020**, *498*, 3995–4004. [[CrossRef](#)]